Journal of Structural Geology 179 (2024) 105042

Contents lists available at ScienceDirect

Journal of Structural Geology

journal homepage: www.elsevier.com/locate/jsg

Origin of oblique structures controlled by pre-tectonic thickness variations in frictional and salt-bearing fold-and-thrust belts: Insights from analogue modelling

Pablo Santolaria [a,*], Esther Izquierdo-Llavall [b], Ruth Soto [b], Teresa Román-Berdiel [c], Antonio Casas-Sainz [c]

[a] Department de Dinàmica de la Terra i de L'Oceà, Facultat de Ciències de la Terra, Institut de Recerca Geomodels, Universitat de Barcelona (UB), Barcelona, Spain
[b] Instituto Geológico y Minero de España, CSIC, Unidad de Zaragoza, Zaragoza, Spain
[c] Departamento de Ciencias de la Tierra, GEOtransfer (IUCA), Universidad de Zaragoza, 50009 Zaragoza, Spain

ARTICLE INFO

Keywords:
Analogue modelling
Oblique structures
Thickness changes
Thrust wedges
South pyrenean central salient
Keping Shan fold-and-thrust belt

ABSTRACT

This work includes, first, a synthesis of experimental analogue modelling programs assessing the influence of along-strike thickness variations in the development of oblique structures in fold-and-thrust belts. As a second part, we present a new experimental program testing, systematically, the influence of tapered décollement-cover thrust wedges.

Previous experiments show that frictional, brittle models feature numerous, short-wavelength structures where the cover is thinner. Deformation fronts are totally or locally oblique to the backstop when the cover thinning is progressive or sharp, respectively. Low (<30°) or higher structural obliquities occur when thickness variations are progressive or sharp, respectively. The addition of a basal or intermediate décollement, commonly entails the transference of deformation towards its external pinch-out. Consequently salients occur and transfer zones and oblique structures form over décollement boundaries. Their location and orientation strongly depend on the pre-compressional shape of the décollements. Furthermore, as demonstrated by our modelling results, tapered brittle covers over viscous décollements result in asymmetric thrust wedges formed by structures that end or change their vergence laterally, resulting in obliquities generally <30°.

Two natural case studies, showing strong (South Pyrenean Central Salient) or moderately oblique (Keping Shan fold-and-thrust belt) structures are revisited and compared to the described analogue models.

1. Introduction

Oblique and lateral structures are very common in compressional settings (e.g., Dahlstrom, 1970; Thomas, 1990; McClay, 1992; Soto et al., 2002; Morley, 2009) and their origin is interpreted (i) considering compression/shortening directions perpendicular to each structural trend (see, e.g., Capote et al., 2002; Liesa and Simón, 2009) or (ii) considering controlling factors such as basement geometry, the mechanical stratigraphy or changes in thickness of the sedimentary pile, etc. (Macedo and Marshak, 1999; Marshak, 2004; Mora et al., 2010; Schori et al., 2021). Deciphering their origin requires a proper 3D knowledge of their geometry and kinematics and the integration of paleomagnetic, structural and sedimentological information (e.g., Craddock et al., 1988; McCaig and McClelland 1992; Sussman et al., 2004; Mochales et al., 2012; Muñoz et al., 2013; Valcárcel et al., 2015; Rodríguez-Pintó et al., 2016). Despite the good number of studied examples worldwide, the origin of many oblique structures is far from being well established. Geometry and dynamics of convergent margins (e.g. subduction zones of the Pacific ring, Yamaoka et al., 1986; Fukao et al., 1987; the Alpine-Himalayan system, Sobel et al., 2013; Bosboom et al., 2014; Crespo-Blanc et al., 2016; Cifelli et al., 2016), long-lived crustal discontinuities at the orogen scale (e.g. Zagros, Mobasher and Babaie, 2008; Lacombe et al., 2011; Joudaki et al., 2016), inherited basement structures in intra-plate settings (e.g. the Iberian Chain, Casas et al., 1998; Merten et al., 2006), inherited salt-related structures (e.g. Vendeville and Nilsen, 1995; Rowan and Vendeville, 2006; Duffy et al.,

* Corresponding author.
E-mail addresses: p.santolaria.otin@ub.edu (P. Santolaria), e.izquierdo@igme.es (E. Izquierdo-Llavall), r.soto@igme.es (R. Soto), mtdjrb@unizar.es (T. Román-Berdiel), acasas@unizar.es (A. Casas-Sainz).

https://doi.org/10.1016/j.jsg.2023.105042
Received 11 July 2023; Received in revised form 14 December 2023; Accepted 19 December 2023
Available online 24 December 2023

2018; Santolaria et al., 2021a, b), vertical axis rotations (Pyrenees, Dinarès et al., 1992; Soto et al., 2006a; Mochales et al., 2012; Muñoz et al., 2013; Sevier thrust belt, Eldredge and Van der Voo, 1988; Yonkee and Weil, 2015), oblique convergence (e.g., Verkhoyansk and the Carpathians, Linzer, 1996; Linzer et al., 1998; Alps, Thöny et al., 2006; Konstantinovsky, 2007; Pueyo et al., 2007 and references therein) and complex evolutions including more than one of these variables have been invoked as responsible for their origin. Apart from those, lateral thickness variations of the deforming stratigraphic pile also represent a first order parameter controlling their occurrence (e.g., Appalachian Plateau, Davis and Engelder, 1985; Jura, Hindle et al., 2000; Hindle and Burkhard, 1999; Zagros fold-belt, Bahroudi and Koyi, 2003).

Analogue modelling permits the analysis of the influence of isolated parameters on a particular process and has demonstrated, since the 70's, that, among all the possible causes, along-strike thickness and rheological changes in the deforming sedimentary sequence play a major role controlling the formation of oblique structures (e.g., Seely, 1977; Marshak and Wilkerson, 1992; Calassou et al., 1993; Corrado et al., 1998; Macedo and Marshak, 1999; Soto et al., 2002). Rheological variations in the stratigraphic pile can be related to changes in the thickness distribution of sediments and/or to areal changes in the distribution of décollements. Such variations are common features often related to palaeogeographic and palaeoenvironmental differences (e.g., Speed et al., 1984; Morley, 1987), inhomogeneous basement fault networks (e.g., Baars and See, 1968; Thomas, 1986) and salt migration is salt-bearing rifted margins (e.g., Rowan, 2014; Granado et al., 2023). In this latter case, systems subsequently evolve to a panoply of fold orientations during mountain building (Crespo-Blanc et al., 2017; Santolaria et al., 2021b; Jiménez-Bonilla et al., 2022).

After introducing the concept of obliquity in natural fold-and-thrust belts (FTBs) (section 2), we provide a synthesis of previous analogue modelling series involving lateral variations of the deforming stratigraphy and/or an uneven distribution of salt-analogue décollements (section 3). Note that works focusing on other parameters that induce oblique structures in FTBs, are not considered in this study. Apart from previous modellers contributions (section 4), we present our new contribution (section 5), that involves thrust wedges featuring laterally tapered brittle-ductile sequences, a parameter never systematically tested before. Comparisons between models and two natural examples (South Pyrenean Central Salient and Keping Shan FTB, in NW China) highlight the major role played by along-strike thickness variations on the development of oblique structures as well as on their overall geometry.

2. Obliquity types in nature

Obliquity in FTBs can be defined qualitatively as the lack of parallelism between structures or the lack of parallelism of one or several structures with the main trend of the chain or its backstop. We will here adopt the latter definition, that can be quantitatively understood as the angle between the backstop of the chain and each individual or each set of oblique structures. Obliquity in FTBs can result from different mechanisms which can be grouped in: i) orogen-driven obliquities (Fig. 1A–D), ii) those related to different shortening directions with time, lateral variations in the amount of shortening and the obliquity between plate margins and the convergence direction (see e.g., Capote et al., 2002; Liesa and Simón, 2009; Lacombe et al., 2011) or iii) obliquities that indirectly formed under the effect of a linear backstop/plate boundary as the original deformation engine, with (Fig. 1E) or without (Fig. 1F) vertical axis rotations, and resulting from orthogonal convergence (Soto et al. 2002, 2003, 2006a, 2006b; Storti et al., 2007; Chattopadhyay et al., 2014; Sadeghi et al., 2016). In this paper we will focus on the study of oblique structures of this third scenario (Fig. 1E and F). This scenario embraces progressive (Fig. 1E) and primary (Fig. 1F) arcs (Weil and Sussman, 2004). Nevertheless, it must be recognized that particularly interesting cases arise when considering

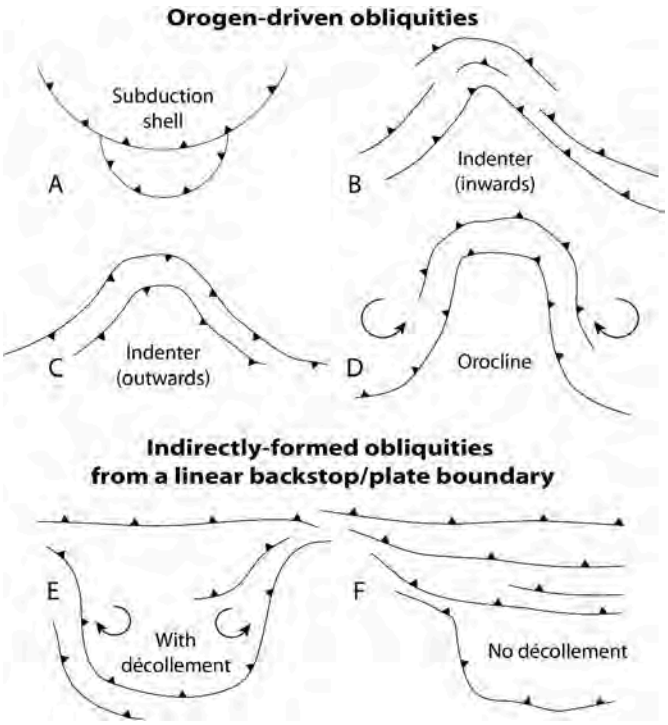

Fig. 1. Sketch showing the different scenarios associated with the formation of oblique: A) Orogen-driven obliquities responding to the arc-shaped geometry of subduction zones or B, C) the varying shape of the plate margins/backstop of the orogenic belt (Zweigel, 1998; Zweigel et al., 1998; Macedo and Marshak, 1999; Keep, 2000; Crespo-Blanc and González-Sánchez, 2005; Rosenberg et al., 2007; Crespo-Blanc, 2008; Reiter et al., 2011, Jiménez-Bonilla et al., 2020, among others), D) oroclinal bending (Weil and Sussman, 2004; Gutiérrez-Alonso et al., 2012 and references therein) and E) and F) obliquities form indirectly from linear backstops or plate boundaries.

arched backstop geometries (e.g. Jiménez-Bonilla et al., 2020). In these cases, normal, strike-slip and reverse faulting co-exist, something that it is not easy to observe in the simpler models related to thickness variations, that are the main objective of this work.

In their turn, those obliquities formed under the effect of a linear backstop/plate boundary, can be divided into: i) thin-skinned oblique structures, those related to regional ductile décollements conditioning the decoupling between the deformation of the basement and the cover, and ii) thick-skinned oblique structures, which involve basement units. The obliquity of thin-skinned oblique structures is strongly conditioned by the areal distribution and the geometry of the décollement and the ratio between the décollement and overlying cover thicknesses. Structures usually show moderate to strong angles to the primary parallel-to-the-orogen structures (e.g. detached cover of the Southern Pyrenees, Soto and Casas, 2001; Oliva-Urcia and Pueyo, 2007; Vidal-Royo et al., 2009; Fernández et al., 2012; Muñoz et al., 2013; the thin-skinned Keping Shan FTB, Allen et al., 1999; Turner et al., 2011).

3. Review of previous experimental settings

In this section we overview analogue experimental programs (considering analogue materials, experimental devices and tested parameters) involving purely contractional models using a linear backstop as deformation mechanism and laterally variable thicknesses of the viscous and/or brittle sequences (Table 1). Therefore, experimental models featuring simple, layer cake stratigraphies (e.g., Costa and Vendeville, 2002), regardless if indenters with different shapes are used (e.g., He et al., 2022), sedimentary wedges trending parallel to the shortening direction (e.g., Smit et al., 2003), inherited connected or isolated salt bodies (e.g., Duffy et al., 2018; Santolaria et al., 2021a,b),

Table 1
Summary of the main characteristics of the models included in this review. The angles between structures and the backstop were roughly defined from the map view photographs of the models included in the considered studies. Note that some works may include different set ups or stratigraphic successions and therefore fit in different model subtypes.

Model types	Model subtype	Backstop geometry	Materials	Brittle cover geometry (along-strike geometry)	Angle of oblique structures to the backstop	References
Brittle wedge with along-strike variations in the backstop/cover thickness ratios (Type A)	**Sharp transition**	Constant thickness	Sand	Sharp thickness changes	30–45	Calassou et al. (1993)
					30–45	Corrado et al. (1998)
					16	Marshak and Wilkerson (1992)
					<23	Marques and Cobbold (2002)
					15–20	Lu et al. (1998)
			Sand and glass microbeads	Sharp thickness changes	16, 27, 35	Sun et al. (2016)
		Sharp thickness changes	Sand	Constant thickness	15–60	Marshak et al. (1992)
						Macedo and Marshak (1999)
	Gradual transition	Constant thickness	Sand	Tapered	30	Soto et al. (2002)
					30	Soto et al. (2003)
			Sand and glass microbeads	Tapered	0–50	Turrini et al. (2001)
			Sand, glass-powder and glass microbeads	Tapered	25	Philippe et al. (1998)
		Tapered	Sand	Constant thickness	10–15	Soto et al. (2006b)
Presence of salt-analogue décollements (Type B)	**Laterally discontinuous décollements**	Constant thickness	Sand and basal silicone	Tapered	30	Storti et al. (2007)
			Sand and basal silicone (interbedded in Corrado et al., 1998; and corundum in Ellis et al., 2004)	Sharp thickness changes	35–70	Corrado et al. (1998)
					15–90	Cotton and Koyi (2000)
					24–45	Lickorish et al. (2002)
					15–40	Luján et al. (2003)
					10–90	Bahroudi et al. (2003)
					–	Ellis et al. (2004)
					15–60	Vidal-Royo et al. (2009)
					10–90	Li and Mitra (2017)
			Corundum and basal silicone	Sharp thickness changes	45–55	Schreurs et al. (2001)
			Sand and several silicone layers	Sharp thickness changes	No plain view	Sans (2003); Koyi and Sans (2006)
					No plain view	Bonini (2007)
					15, 23, 40	Santolaria et al. (2015)
			Sand, basal glass microbeads décollements and interbedded silicone	Sharp thickness changes	20–90	Borderie et al. (2018)
					20–50	Vendeville et al. (2017)
			Sand and basal vermiculite	Sharp thickness changes	45	Macedo and Marshak (1999)
			Sand a several glass microbeads layers	Sharp thickness changes	20–30	Ravaglia et al. (2004)
					30, 40	Ravaglia et al. (2006)
			Sand, interbedded microbeads décollement and basal silicone	Sharp thickness changes	20–30	Farzipour-Saein and Koyi (2014)
			Sand and aluminum microspheres	Gradual thickness changes	10–30	Bigi et al. (2009)
			Sand and basal silicone	Tapered	10	Ter Borgh et al., 2011
	Laterally tapered décollements	Constant thickness	Sand and silicone	Constant thickness	10	Calassou et al. (1993)
				Tapered	30	Lickorish et al. (2002)
				Tapered (+ tapered basal silicone plate)	<30	Izquierdo-Llavall & Casas Sainz (2012); This study
			Sand and silicone-iron powder mixture	Tapered	50–90	Van der Werf et al. (2023)

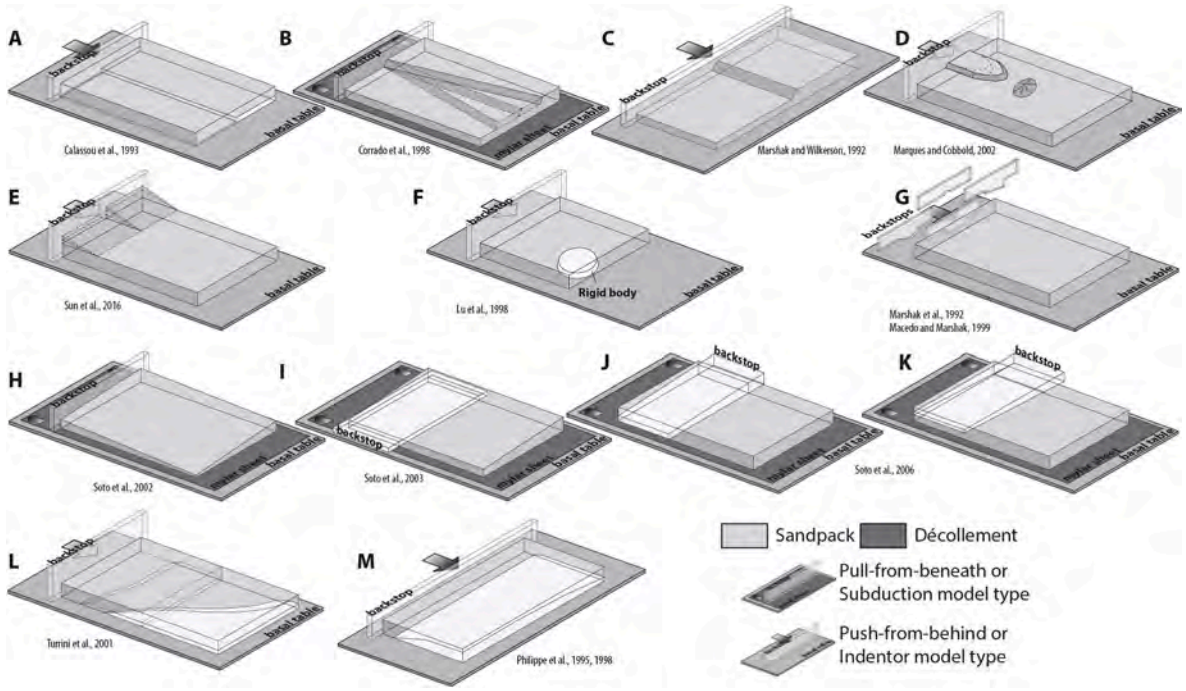

Fig. 2. Synthetized set-ups and model types for series of analogue models regarding brittle wedges with along-strike variations in the backstop/cover thickness ratios (Type A models, see Table 1). Sketches do not represent actual dimensions and geometries of the original experiments but simplified versions of them (check original reference for further information). Continuous to dashed lines refer to different tested scenarios of specific experimental programs.

surface processes (e.g. Storti and McClay, 1995; Wu and McClay, 2011; Pla et al., 2019), multiple deformation phases involving extension or multidirectional convergence (Cerca et al., 2004; Dooley and Hudec, 2020; Soto et al., 2020; Ferrer et al., 2022; Miró et al., 2022; Wilson et al., 2023) and orogen-driven oblique structures (e.g. Lickorish et al., 2002; Jiménez-Bonilla et al., 2020) are out of the scope of this synthesis. Centrifuge models dealing with this issue (Santolaria et al., 2014, 2022) but using different combinations of sands and polymers will not be considered, either.

3.1. Materials

Suitability of each analogue material to simulate rocks in nature is discussed in detail in the works cited in Table 1. For detailed descriptions and mechanical analyses of analogue modelling materials see e.g., Lohrmann et al. (2003), Panien et al. (2006), Klinkmüller et al. (2016), Schellart and Strak (2016), Rudolf et al. (2016) and Montanari et al. (2017). Natural prototypes (see section 7) that inspired or are used to establish experiment-to-nature comparison regard oblique structures in the upper crust. To simulate brittle, upper crustal rocks, modelers mostly use dry aeolian quartz sand since it obeys a Mohr-Coulomb criterion of failure (Hubbert, 1951; Mandl et al., 1977; Krantz, 1991; Schellart, 2000; Lohrmann et al., 2003; Panien et al., 2006; Klinkmüller et al., 2016; Schellart and Strak, 2016). Sand shows low cohesion, density from 1.3 to 1.6 g/cm^3, grain size between 0.1 and 0.4 mm and internal friction angle between 30° and 37.5° (Rosenau et al., 2018; Willingshofer et al., 2018; Zwaan et al., 2018; Román-Berdiel et al., 2019; Warsitzka et al., 2019 and references in Table 1). Schreurs et al. (2001) and Ellis et al. (2004) used corundum powder, which has a higher density (ca. 1.9 g/cm^3). As an exception, Marshak and Wilkerson (1992), Marshak et al. (1992) and Macedo and Marshak (1999) slightly damped the sand to impart an apparent cohesiveness. Some experimental series simulated the ductile or viscous behaviour of specific rocks in the upper crust, namely evaporites or water-saturated clay-rich units. Among evaporites, anhydrite should be excluded since its density (up to 3.0 g/cm^3) is higher than most carbonate and detrital rocks which may compromise scaling ratios. All of the brittle-ductile summarized experiments simulate stratigraphic piles where décollement is lighter than the brittle cover. Evaporites or water-saturated clay-rich units commonly act as décollements and are simulated by silicone putty composed of polydimethylsiloxane (PDMS). SGM-36 and Rhodia silicone 7007 are the most extensively used types. Lickorish et al. (2002) used Silbione Gomme A0009 and Li and Mitra (2017) used a silicone gel. Van der Werf et al. (2023) used also PDMS silicone but mixed with iron powder. These silicones have a Newtonian behaviour (the relationship between stress and strain rate is linear) for strain rates lower than 3×10^{-3} s^{-1} (Weijermars, 1986; Weijermars and Schmeling, 1986; Rudolf et al., 2016), that are within the ranges applied in most of the models. Their viscosity varies between $1.2{\cdot}10^4$ and $6{\cdot}10^5$ Pa s at room temperature and their density is approximately 0.987 g/cm^3 for the SGM-36 and between 1.14 and 1.3 g/cm^3 for the Rhodia silicone. The PDMS-iron mixture used by Van der Werf et al. (2023) attained a density of 1.241 g/cm^3. Other materials used to simulate weak layers and/or frictional detachment levels include glass powder (Philippe et al., 1998), glass microspheres (Philippe et al., 1998; Ravaglia et al., 2004; Sun et al., 2016; Vendeville et al., 2017; Borderie et al., 2018) and aluminium microspheres (Bigi et al., 2009). Vermiculite (density 0.29 g/cm^3) has been used side by side with sand (Macedo and Marshak, 1999) to simulate the effect of cover strength variations.

3.2. Experimental devices

Two experimental devices have been used (Figs. 2 and 3): (i) the push-from-behind or indentation model device (moving backstop), where analogue material lies on wooden or aluminium-topped tables, sometimes topped with glued sand to increase the basal friction (Vidal-Royo et al., 2009), and (ii) the pull-from-beneath or subduction model device (fixed backstop) where the model lies on basal sheets such as drafting films or mylar sheets. Models can be confined, unconfined or semiconfined (either the lateral or the forelandward walls are absent). Moving or fixed backstops can be deformable, usually sand, Bigi et al. (2009) or rigid (wood, PVC). The geometry of the backstop is also

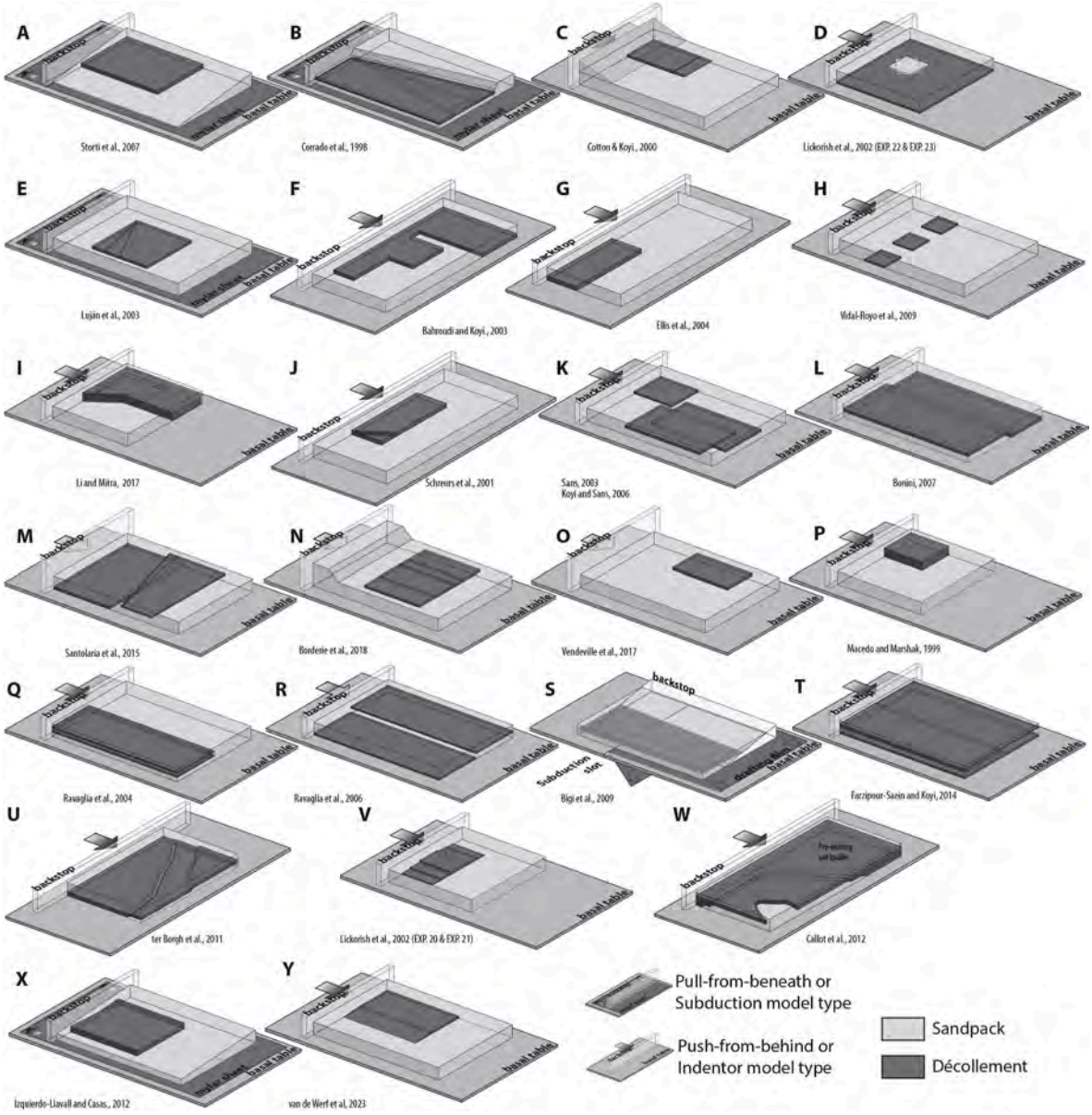

Fig. 3. Synthetized set-ups and model types for series of analogue models involving the presence of laterally variable salt-analogue décollements (Type B models, see Table 1). Sketches do not represent actual dimensions and geometries of the original experiments but simplified versions of them (check original reference for further information). Continuous to dashed lines refer to different tested scenarios of specific experimental programs.

variable: straight and vertical (Corrado et al., 1998; Cotton and Koyi, 2000; Schreurs et al., 2001; Soto et al., 2002; Bahroudi and Koyi, 2003; Luján et al., 2003; Sans, 2003; Ravaglia et al., 2004, 2006; Bonini, 2007; Storti et al., 2007; Vidal-Royo et al., 2009; Santolaria et al., 2015; Sun et al., 2016; Vendeville et al., 2017; Borderie et al., 2018; this study), wedge-shaped (Calassou et al., 1993), flat-lying, with a constant thickness (Soto et al., 2003), tapered (Soto et al., 2006b) or other geometries (Macedo and Marshak, 1999; Philippe et al., 1998; Marshak et al., 1992).

3.3. Tested parameters

The challenge of interpreting analogue model results lies in the number of different parameters operating simultaneously. In the laboratory, oblique structures in FTBs has often been analysed using setups focused on inferring the effect of along-strike thickness changes and/or rheological variations within the silicone-sand pack. Such variations can be achieved by (i) varying the relative thickness of the backstop with respect to the sand pack, (ii) changing the thickness of the sand pack itself, and/or (iii) including salt-analogue décollements with different plan-view geometry, stratigraphic distribution and/or thicknesses. Accordingly, we classify models as 1) Type A, brittle wedges with along-strike sharp or gradual variations resulting from backstop or sedimentary pack thickness variations (Fig. 2) and 2) Type B, brittle-ductile wedges that involve the presence of laterally variable salt-analogue décollements that may terminate sharply, leading to abrupt rheological discontinuities or gradually, if tapered décollements are considered (Fig. 3). In Type A experiments, lateral variations of the backstop/cover thickness ratio (Fig. 2) are frequently achieved by means of stepped bases (Fig. 2A, Calassou et al., 1993, Fig. 2G, Marshak et al., 1992, Macedo and Marshak, 1999, Fig. 2F, Lu et al., 1998, Fig. 2M, Philippe et al., 1998, Fig. 2L, Turrini et al., 2001) or tapered backstops (Fig. 2J and K, Soto et al., 2006b). Other ways to obtain thickness variations consist of maintaining a horizontal base vs. a tilted or offset top of the model (Fig. 2B and Corrado et al., 1998, Fig. 2C, Marshak and Wilkerson, 1992, Fig. 2E, Sun et al., 2016, Fig. 2L, Turrini et al., 2001, Fig. 2H,

Soto et al., 2002, Fig. 2I, Soto et al., 2003). Some brittle-wedge models also include low-friction detachments (glass-microbeads) at the base of the deforming material (Philippe, 1995; Philippe et al., 1998; Sun et al., 2016).

Most brittle-ductile Type B wedges feature sharp lateral variations of the analogue materials (Fig. 3). They show a basal horizon with one or more rheological discontinuities where sand passes laterally to silicone (or glass microbeads or vermiculite) (Fig. 3A, Storti et al., 2007, Fig. 3C, Cotton and Koyi, 2000, Fig. 3D, V, Lickorish et al., 2002, Fig. 3E, Luján et al., 2003, Fig. 3F, Bahroudi and Koyi, 2003; Fig., 3G, Ellis et al., 2004, Fig. 3H, Vidal-Royo et al., 2009, Fig. 3I, Li and Mitra, 2017, Fig. 3J, Schreurs et al., 2001, Fig. 3K, Sans, 2003; Koyi and Sans, 2006, Fig. 3P, Macedo and Marshak, 1999, Fig. 3Y, Van der Werf et al., 2023) and/or an interbedded décollement (Fig. 3B and Corrado et al., 1998, Fig. 3K, Sans, 2003 and Koyi and Sans; Fig. 3Q and Ravaglia et al., 2004, Fig. 3R, Ravaglia et al., 2006, Fig. 3L, Bonini, 2007, Fig. 3S, Bigi et al., 2009, Fig. 3M, Santolaria et al., 2015, Fig. 3O, Vendeville et al., 2017, Fig. 3N, Borderie et al., 2018).

Thus, in compressional settings, the principal parameters tested in the laboratory to infer the origin of oblique structures are i) the presence of lateral vertical offsets in a non-deformable basement (Calassou et al., 1993) or lateral sharp offsets of the cover top surface (Marshak and Wilkerson, 1992; Corrado et al., 1998; Marques and Cobbold, 2002; Sun et al., 2016), ii) the relative angles between the backstop and a linear thickness discontinuity in a sandy cover (Corrado et al., 1998), iii) the obliquity, with respect to the transport direction, of a discontinuity simulating a platform-basin transition (Philippe et al., 1998; Turrini et al., 2001), iv) the lateral thickness variations of the cover in mono-vergent (sand pack, Soto et al., 2002; silicone-sand pack, Storti et al., 2007; Ter Borgh et al., 2011) and doubly-vergent thrust wedges (Soto et al., 2003), v) the along-strike tapering of the backstop in doubly-vergent thrust wedges (Soto et al., 2006b), vi) different basin shapes (Marshak et al., 1992; Macedo and Marshak, 1999), vii) the occurrence of adjacent viscous and frictional décollements whose boundaries vary in terms of geometry, position and angle relative to the shortening direction (Macedo and Marshak, 1999; Cotton and Koyi, 2000; Schreurs et al., 2001; Lickorish et al., 2002; Luján et al., 2003; Bahroudi and Koyi, 2003; Sans, 2003; Ellis et al., 2004; Koyi and Sans, 2006; Bonini, 2007; Vidal-Royo et al., 2009; Li and Mitra, 2017), viii) the gradual along-strike thinning of décollement levels (Lickorish et al., 2002; Izquierdo-Llavall and Casas Sainz, 2012; Callot et al., 2012; Van der Werf et al., 2023) and ix) the occurrence of interbedded viscous (Corrado et al., 1998; Sans, 2003; Ravaglia et al., 2004; Koyi and Sans, 2006; Santolaria et al., 2015; Vendeville et al., 2017; Borderie et al., 2018) or semi-frictional (Ravaglia et al., 2004, 2006; Bigi et al., 2009; Farzipour-Saein and Koyi, 2014) horizons within the sand pack.

4. Previous modelers' contributions

The main observations and results derived from the two previously introduced brittle and brittle-ductile wedge experiments (Types A and B in Figs. 2 and 3, respectively) are here summarized (see also Table 1). We focus on the factors that, among the tested parameters, triggered the development of oblique structures.

4.1. Brittle wedges with along-strike variations in the backstop/cover thickness ratios (Type A)

4.1.1. Sharp thickness ratio variations

A sharp along-strike thickness variation in the pre-contractional sequence strongly conditions the resulting structures, regardless of if variations are created by a vertical step in the basal plate (Lu et al., 1998, Fig. 2F; Calassou et al., 1993, Fig. 2A and 4A) or by decreasing the sand pack thickness over a horizontal basal plate (slope at the sand surface, Marshak and Wilkerson, 1992; Corrado et al., 1998; Marques and Cobbold, 2002; Sun et al., 2016, Fig. 2B, C, D, E and 4B, C). Results are very similar in these models, where only a brittle cover is considered (homogeneous sand pack): structures are not cylindrical and a major bend develops (i) above the basement offset, forming a transfer zone with limited extension (Calassou et al., 1993, Fig. 4A) or (ii) in the thin compartment either next to the slope marking the cover thickness variation (Corrado et al., 1998) or across the whole thin domain (Sun et al., 2016, Fig. 4B). Deformation is strongly asymmetric, both in time and space, with thrusts emerging first in the thin compartment and later in the thick one, where a lower number of thrusts develop, and the deformation front propagates farther from the backstop. The geometric and kinematic evolutions do not depend on the basal friction (Calassou et al., 1993 tested two different basal friction angles of 18° and 27°) nor the orientation of the thickness change slopes with respect to the shortening direction (Corrado et al., 1998, tested three different angles of 60°, 90° and 120°). Sun et al. (2016) simulated along-strike thickness changes by means of two sand wedges, restricted to the area closest to the backstop (Fig. 2E), that showed different across-strike slope angles and maximum heights. In these set-ups, oblique structures propagated into the foreland farther than the area displaying the thickness change (Fig. 4B) and the obliquity between them and the shortening direction was higher for the larger along-strike thickness changes and for the stronger across-strike slope differences. Marques and Cobbold (2002) simulated along-strike thickness changes by means of an irregular topography, either by creating thicker/thinner zones in the central area of the model next to the backstop, or thicker zones in areas farther away from the backstop (Fig. 2D). In these set-ups, accreting thrusts tended to be arcuate, (i) convex towards the foreland, ahead of the initially high-topography area; and (ii) concave towards the foreland, around the initially low-topography area (Fig. 4C). The presence of a circular basement high (Lu et al., 1998, Fig. 2F) delays the propagation of the deformation front forelandwards of the high, but with enough shortening, the deformation front advances more than in adjacent areas. Consequently, a curved deformation front forms.

The effect of along-strike sharp changes in backstop geometry (Macedo and Marshak, 1999, Fig. 2G) can be considered analogous to that of along-strike thickness variations in the cover: the sand pack pushed by the irregular backstop glides over an undeformed sand package, which is equivalent to a shaped basal, undeformable plate. Changes of the geometry of the backstop result in thrust systems mimicking the shape of the backstop in map view (Fig. 4D–G). The thrust wedge formed by the thinner backstop is relatively narrow and contains closely spaced faults, whereas the thrust system formed by the thicker backstop is wider and consists of more widely spaced structures forming a salient. Fault traces in this salient are arcuate and connect to thrusts in the narrow wedge. Structures in the transition area are oblique and locally accommodate strike-slip movements. The strike and extent of these oblique structures depends on the backstop geometry.

4.1.2. Gradual thickness variations

Along-strike gradual changes in the thickness of pre-compressional units also induce a non-cylindrical growth of the thrust wedges (Philippe et al., 1998; Soto et al., 2002; Soto et al., 2003, Fig. 4H and 5A, B). Thrusts emerge first in the thinner part of the models and then propagate laterally into the thicker parts, and thrust sheets are more abundant but narrower in the thinner domains and scarcer but wider in the thicker domains, where the deformation front is at higher distance from the backstop. Synchronous thrusting characterizes the evolution of the thicker areas while "true piggyback thrusting" occurs in the thinner sectors (i.e. all the shortening is accommodated by the frontal thrusts whereas inner thrusts become inactive, Soto et al., 2002). These thrusts run obliquely to the backstop almost along the entire model (Fig. 5), defining oblique domains that are commonly wider than those developed in the models where thickness changes are sharp.

The geometry of the thickness transition strongly controls the structural relay between thinner and thicker domains. Thickness changes, achieved by a longitudinal bend on a basal rigid plate (Philippe

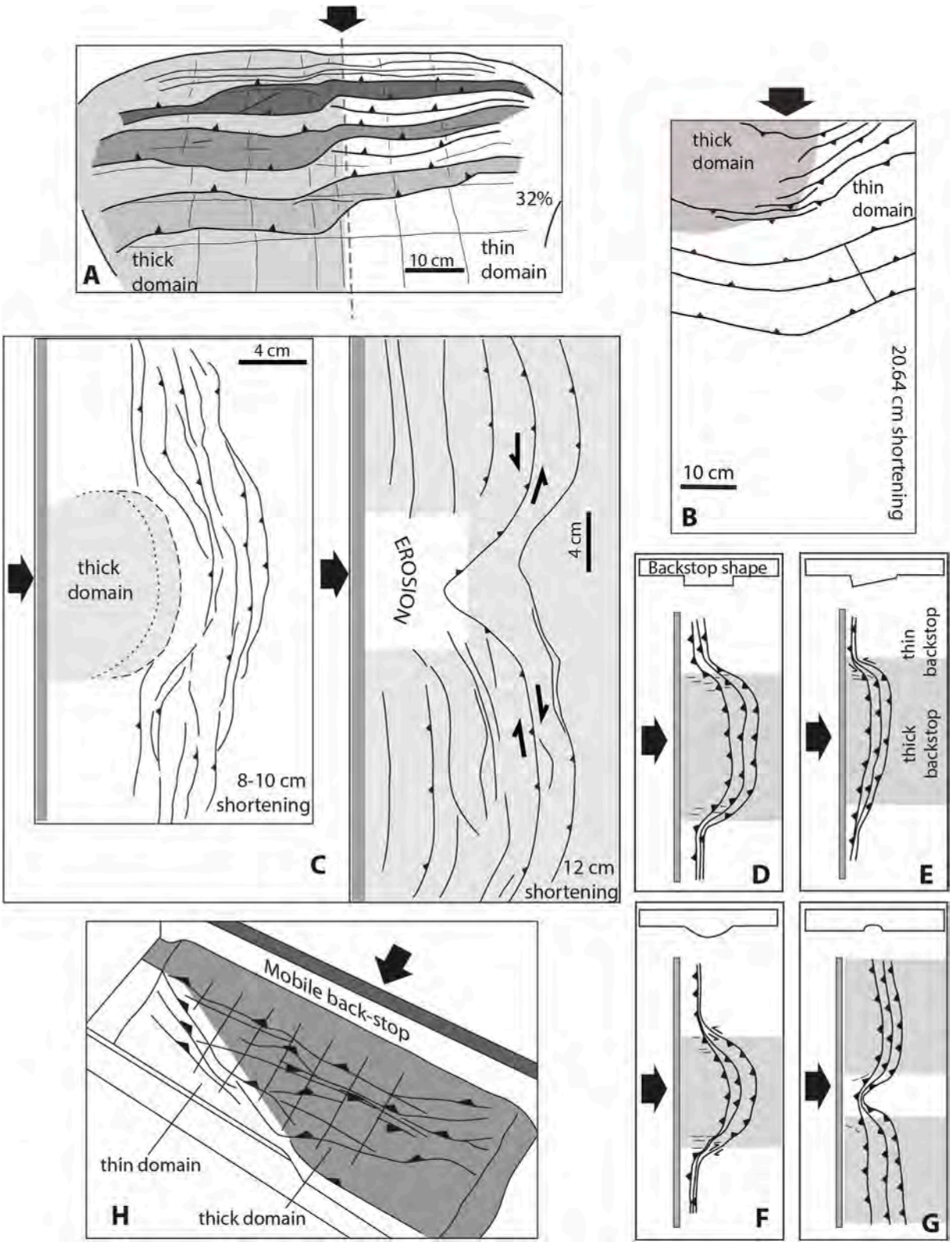

Fig. 4. A, B and C) Line drawing of the plan view deformation– of three experiments with sharp thickness variations: A) sharp transition created by a vertical step in the basal plate, model constituted by a single brittle sand layer (modified from Calassou et al., 1993); B) along-strike thickness changes by means of two sand wedges, restricted to the model area closest to the backstop (modified from Sun et al., 2016); C) along strike thickness variation are created by means of thicker/thinner local zones next to the backstop (based on Marques and Cobbold, 2002); D to G) Line drawing of plan views of the final stages of four sandbox experiments simulating formation of basin-controlled salients: D) symmetric rift; E) asymmetric rift; F) spoon-shaped basin; G) structural high (modified from Macedo and Marshak, 1999). H) Line drawing of an oblique view of the final deformation stage in the model by Philippe et al. (1998) where the thickness change in the cover sequence is gradual and was achieved through a longitudinal bend on a basal rigid plate. Initial set-ups are sketched in Fig. 2.

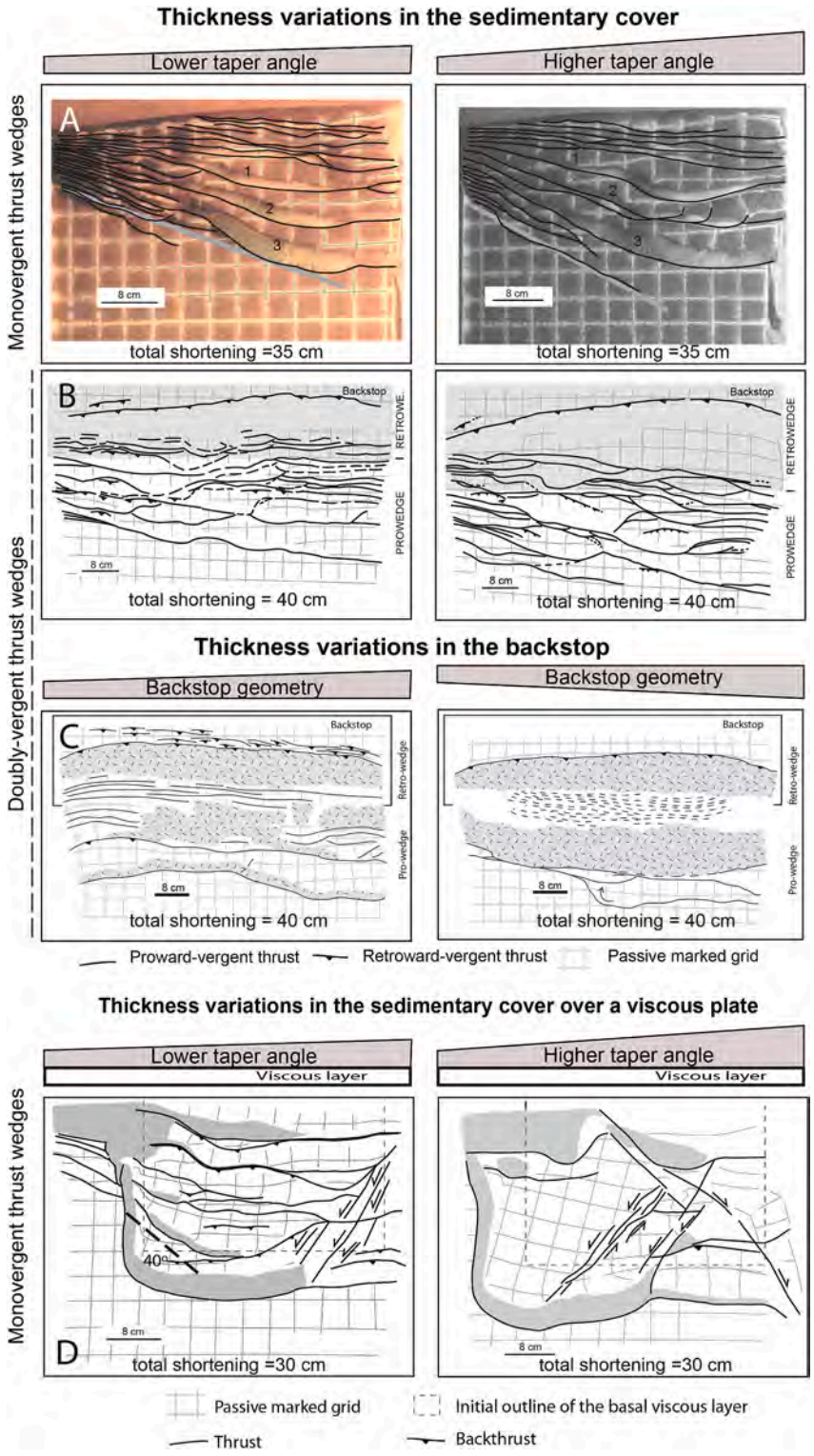

Fig. 5. Line drawings of model top views at final shortening stages. Analogue models belong to four different experimental series displaying gradual, along-strike thickness variations in the initial sedimentary cover (A, B and D) or in the backstop (C). They consist of a sand pack (A, B, C) or a sand pack overlying a constant-thickness, basal viscous décollement (D). A) Monovergent sand wedges with varying taper angle (Soto et al., 2002); B) Doubly-vergent sand wedges with varying taper angle (Soto et al., 2003); C) Doubly-vergent orogenic wedges with an along-strike tapered backstop (Soto et al., 2006b). Backstops showed: 1) a horizontal basal surface and a laterally tapered upper surface or (2) a laterally tapered basal surface and a horizontal upper surface. D) Monovergent sand wedges with varying taper angle, overlying a basal silicone plate (Storti et al., 2007). Boundaries of this silicone plate are indicated. Initial set-ups are sketched in Fig. 2.

et al., 1998, Fig. 2M), result in the development of prominent oblique ramps over the basement flexure (Fig. 4H). These structures begin to form in the early stages of shortening and compartmentalized the model into a thinner block and a thicker block where frontal ramps dominate (i.e. thrusts are parallel to the backstop). Nevertheless, model geometries significantly differ when thickness variations are simulated by means of a wedged sand pack showing a constant taper angle (Soto et al., 2002, 2003). These geometries lead to a diffuse structural transition between thinner and thicker areas. This fact materializes in highly segmented orogenic wedges displaying anastomosing geometries and frequent lateral and oblique ramps (Fig. 5A) whose outer envelope strikes obliquely to the backstop. The higher the taper angles the more oblique deformation fronts are (e.g. taper angles of 3.5 and 5.5° involves obliquities of 20 and 30° with regard to the backstop, respectively, Fig. 5A).

In doubly-verging experimental wedges, progressive tapering of the cover produces strongly asymmetric thrust systems displaying a wider and highly segmented pro-wedge and a narrower retro-wedge where deformation progresses by activating a single, main back-thrust (Fig. 5B) (Soto et al., 2003). Deformation fronts in both the pro-wedge and the retro-wedge are oblique to the backstop but at an angle that is smaller than that obtained in the mono-vergent experiments (compare Fig. 5A and B). Similar thrust wedge geometries can be obtained by using vertical and along-strike tapered backstops that deform a constant-thickness cover sequence (Soto et al., 2006b, Fig. 5C).

Turner et al. (2010) study the formation of oblique structures in more complex scenarios that combine a non-horizontal basement topography and a pre-deformation wedge-shaped cover. Basement topographies include frontal and oblique ramps combined in different ways and located over a horizontal or inclined (6°) basal plate (Fig. 2L). Moreover, models are constructed with inhomogeneities in the mechanical stratigraphy (i.e., one or more layers of glass microbeads between alternating layers of differently coloured quartz sand). The inhomogeneous mechanical stratigraphy allowed simultaneous folding and thrusting at deep and shallow levels, and in general, results indicate that oblique faults develop and mimic the basement geometry.

4.2. *Brittle-ductile wedges with laterally variable salt-analogue décollements (Type B)*

4.2.1. *Laterally discontinuous décollements*

Many works have investigated the structural variations in analogue models caused by areas with viscous décollements (viscous domains) and without it (frictional domains). In general, these models show lower taper angles and deformation fronts propagates faster and farther above the viscous layer (Fig. 6). As a result, an inflection forms above the frictional/viscous domain boundary (Fig. 6A), leading to surface geometries similar to those obtained in sand packs displaying sharp thickness changes (Fig. 4A). In the frictional part, increasing shortening is accommodated by a piggy-back imbricate, foreland-verging thrusts system. Simultaneously, doubly-vergent thrust systems developed above the viscous décollement (Fig. 6A, Cotton and Koyi, 2000).

The geometry and kinematic evolution of the inflection zones between viscous and frictional domains depend on the basal viscous layer shape as many works highlight, where authors have frequently tried to reproduce the particular conditions of the studied geological settings (Schreurs et al., 2001; Bahroudi and Koyi, 2003; Luján et al., 2003; Sans, 2003; Ellis et al., 2004; Koyi and Sans, 2006; Vidal-Royo et al., 2009, Li and Mitra, 2017, among others). Folds and thrusts tend to localize over the silicone plate boundaries parallel or oblique to them (Fig. 6). Different obliquities have been tested for both the lateral and hinterland boundaries of the décollements. When lateral silicone boundaries are parallel to the shortening direction, lateral ramps are frequent (Fig. 6A, Cotton and Koyi, 2000; Li and Mitra, 2017), whereas when they strike obliquely (35° from the shortening direction in Schreurs et al., 2001, Fig. 6B), oblique thrust ramps formed (Li and Mitra, 2017). Varying angles between the strike of the hinterland-wards silicone boundary and the backstop (0°, 15°, 30° and 45°, see Fig. 3E, Luján et al., 2003) cause a major asymmetry on the resulting 3D structure of FTBs: at lower angles (0–15°) a main, oblique structure develops, parallel to the silicone boundary, whereas intermediate (30°) and higher (45°) angles enhance the development of segmented structures, running parallel to the silicone boundary or the backstop, respectively. If the inner limit of the silicone plate trends perpendicular to the shortening direction and the outer limit depicts a convex shape (Lickorisch et al., 2002; their experiment 20, Fig. 3V), a pronounced salient grows parallel to the silicone convexity. Upon further shortening, the salient is incorporated to the advancing front.

When there is a sharp, along-strike thickness variation in the brittle sequence, the presence of a viscous layer alters the above-described patterns (see section 4.1.1). When a viscous décollement is interlayered only in the thinner domain (Corrado et al., 1998), thrusts are rectilinear in the thick compartment but become arcuate in the thin one (Fig. 6C). At each stage of deformation, fore-thrusts emerge at a larger distance in the thinner domain, conversely to the geometry acquired where only sand was present.

The location of the basal silicone plate within the model also influences the overall geometry of thrust systems: when it is in a central position (Fig. 6D, Luján et al., 2003), foreland-verging (frictional) domains bound a central, doubly verging and rather symmetrical (viscous) domain. As a rule, well developed thrust salients over the viscous domains characterize the final stages of all experiments (Fig. 6D). More complex geometries of the basal viscous layer have been explored by Bahroudi and Koyi (2003) and Vidal-Royo et al. (2009) (Fig. 3F, H); two to three basal silicone plates at varying (Bahroudi and Koyi, 2003) or constant (Vidal-Royo et al., 2009) distances from the backstop. This distribution of viscous décollements produces thrust fronts located at variable distances within the model and separated by deflection zones with oblique and lateral structures (Fig. 6E, Bahroudi and Koyi, 2003). When the along-strike distance between basal décollements is tested (Vidal-Royo et al., 2009), there is a critical width for the inter-viscous frictional domains below which oblique structures and deflection zones do not form. Similar results can be obtained by increasing the sand/silicone thickness ratio (Vidal-Royo et al., 2009).

When a basal décollement is disrupted by localized “obstacles”, represented by areas without silicone (Lickorish et al., 2002), the advancing thrust system is blocked. Then, the thrust system propagates forward on either side of the obstacle, whereas, at the edge of the silicone-free zone, lateral or oblique ramps develop (Fig. 6F).

The occurrence of interbedded viscous layers (Farzipour-Saein and Koyi, 2014; Vendeville et al., 2017; Borderie et al., 2018) also triggers: (i) the outward propagation of the deformation front overlying the viscous layer, and (ii) the development of transfer or inflection zones at the boundary between the viscous and frictional domains (Fig. 6G). Yet, influence of basal discontinuities is more significant than the ones related to interbedded décollements (Farzipour-Saein and Koyi, 2014). These experimental series are characterized by more and narrower thrusts in the viscous domains because they affect a thinner sand sequence (Fig. 6G). The influence of multiple detachments levels in the stratigraphic pile has also been analysed, considering sometimes rheological differences between these levels (Sans, 2003; Koyi and Sans, 2006; Bonini, 2007; Santolaria et al., 2015; Pla et al., 2018; 2019). Interference of structures detached over different décollements commonly results in complex deformation patterns. When low frictional granular detachments (glass microbeads, Ravaglia et al., 2004, 2006; Bigi et al., 2009; Farzipour-Saein and Koyi, 2014) are used, thrust salients, inflection zones, braided patterns and oblique thrust ramps also develop at the décollement boundaries but they are not so pronounced as in the models considering viscous décollements. (Fig. 6H).

When models involve a basal viscous décollement underlying a tapered cover, the complexity of the thrust systems significantly increases. These models consisted of a sand pack wider than the

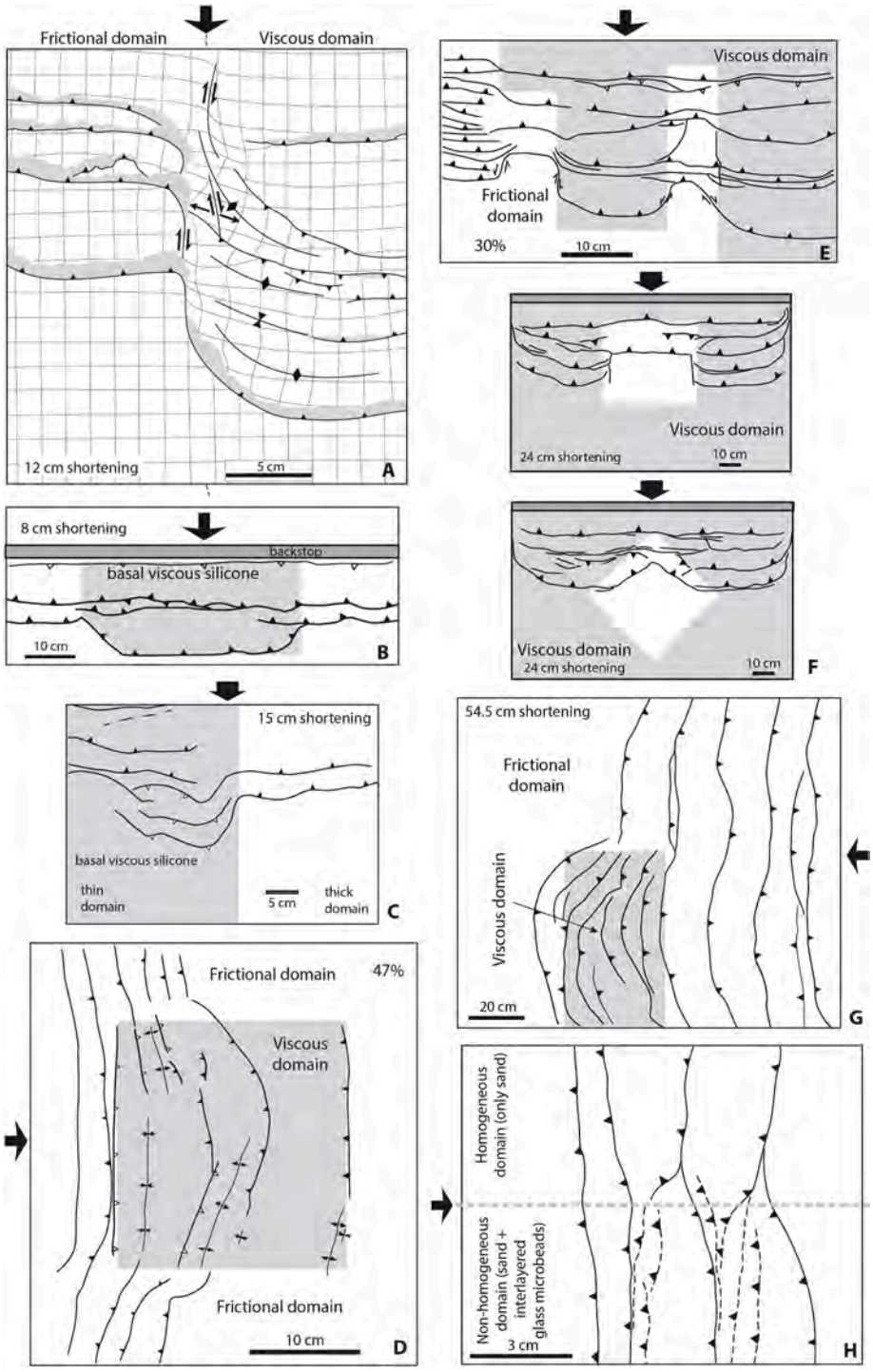

Fig. 6. Line drawing of plan view of the final deformation stage of nine experiments involving viscous (A, B, C, D, E, F and G) and frictional (H) décollements that end laterally. This produces A) a pronounced deflection in the deformation front (modified from Cotton and Koyi, 2000); B) the outward propagation of the deformation front in the central, viscous region with respect to the lateral frictional domains (modified from Schreurs et al., 2001); C) a viscous décollement (silicone putty) is interlayered only in the thinner domain, thrusts are rectilinear in the thick compartment but become arcuate in the thin one (modified from Corrado et al., 1998); D) an arcuate shape deformation front (modified from Luján et al., 2003); E) multiple thrust salient and reentrants related to rheological boundaries (modified from Bahroudi and Koyi, 2003); F) thrust system propagated forward in the sand on either side of the obstacle, whereas, at the edge of the silicone-free zone, lateral or oblique ramps develop (based on Lickorish et al., 2002); G) the forwards propagation of the deformation front above the interbedded viscous layer (drawn from Vendeville et al., 2017); H) braided pattern of thrust fronts; a purely sand sequence lays adjacently to a sand pack with interbedded glass microbeads layers (modified from Ravaglia et al., 2004).

underlying silicone plate and two lateral and frontal frictional domains (Storti et al., 2007). The experiments are characterized by a strong decoupling between the viscous and the lateral frictional domains that connect through strike-slip and transpressional faults or lateral thrust ramps (Fig. 5D). Deformation is commonly localized during early shortening stages along the frontal silicone pinch-out and subsequent out-of-sequence thrusts develop in the inner part of the silicone plate. Transpressional oblique (45–60° to the backstop) faults develop mainly

Table 2
Scaling parameters of the experimental program in this study. *Most of the evaporites with exception of anhydrite since its density can be 3.00 g/cm^3.

Parameter	Model	Nature	Scaling Ratio (model/nature)
Length	0.01 m	500 m	$2{\cdot}10^{-5}$
Gravity	9.8 m/s^2	9.8 m/s^2	1
Density			
Sand/brittle rocks	1.61 g/cm^3	2.70 g/cm^3	0.60
*Silicone/evaporitic décollements**	0.98 g/cm^3	2.20 g/cm^3	0.45
Internal friction angle (*Sand/brittle rocks*)	30°–37°	31°–40° (Bahroudi et al., 2003)	~1
Deviatoric stress ($\sigma = \rho gL$)	96 (*silicone*) −158 (*sand*) Pa	$10.7{\cdot}10^6$ (*evaporites**) $-13.2{\cdot}10^6$ (*brittle rocks*) Pa	$9{\cdot}10^{-6}$-$1.2{\cdot}10^{-5}$ (average $1{\cdot}10^{-5}$)
Viscosity of the ductile layer (μ)	$7{\cdot}10^3$ Pa s (20 °C)	$1{\cdot}10^{18}$ Pa s	$7{\cdot}10^{-15}$
Strain rate ($\varepsilon = \sigma/\mu$)	$1.37{\cdot}10^{-2}$ s (*silicone*)	$1.07{\cdot}10^{-11}$ (*evaporites**)	$1.28{\cdot}10^9$
Velocity ($V = \varepsilon{\cdot}L$)	$4.16{\cdot}10^{-6}$ m/s (1.5 cm/h)	$1.63{\cdot}10^{-10}$ m/s (5 mm/year)	$2.56{\cdot}10^4$
Time ($t = 1/\varepsilon$)	3600 s (1 h)	$4.62{\cdot}10^{12}$ s (0.14 Ma)	$7.8{\cdot}10^{-10}$

localized in the domain where the sand/silicone thickness ratio is higher (Fig. 5D). They connect to, or traverse, previously developed structures forming salients and isolating blocks registering clockwise vertical axis rotations. In general terms, comparison of models with different along-strike sand tapers evidenced that (Fig. 5D): (1) higher taper angles produce an earlier migration of deformation towards the silicone pinch-out, formation of large frontal thrust sheets over the frontal silicone pinch-out, oblique transpressional faults, salients and vertical axis rotation, and (2) shallow along-strike sedimentary tapers favour a higher lateral continuity of structures.

4.2.2. *Laterally tapered décollements*

Experiment by Ter Borgh et al. (2011) shows a stepped décollement topped by a stepped sandy cover. Steps display several inflection points that separate slight to moderate oblique ramps. Basement steps exert a strong effect on the deformation by controlling the location of contractional structures. Lickorish et al. (2002) set up a rectangular silicone zone that thinned laterally and stepwise from the centre to the edges (i.e. thinning is not purely progressive, Lickorish et al., 2002; their experiment 21, Fig. 3V). Thrusts tend to nucleate firstly above the thicker silicone and then propagate laterally with a gradual decrease in spacing, depicting arcuate shapes and recording slight vertical axis rotations. Van der Werf et al. (2023) modelled a tabular décollement that laterally terminates progressively (Fig. 3X). Transfer zones and highly oblique structures form along the décollement pinch-out while moderately oblique structures occur along the tapered décollement area.

Callot et al. (2012) also considered a laterally stepwise thinning silicone layer but, contrary to Lickorish et al. (2002), this layer thinned upwards (Callot et al., 2012; Fig. 3W). Thinning grades from perpendicular to 35° to the shortening direction. The tapered area connects with an area where the viscous layer has constant thickness area and includes pre-existing salt bodies. Silicone layer thickness changes govern the wedge taper, which shows a slightly arcuate shape highly oblique to the lateral thinning trend of the silicone layer.

Izquierdo-Llavall and Casas Sainz (2012) designed an experimental program (Fig. 3Y) testing the along-strike thickness variation of the silicone layer with respect to the overlying brittle cover to conclude that the structural vergence is roughly controlled by the silicone thickness. In their models, the lateral décollement pinch-out is represented by an abrupt rheological transition that led, as discussed before, to a strong decoupling between the viscous and lateral frictional domains. Such models represent the precursor experimental program to the one included in this work and presented in the next section.

5. New models on gradual silicone/sand thickness variations

5.1. *Rationale*

Most of the analogue models summarized in section 4.2 explore the influence of along-strike sharp terminations of weak décollements on the geometry of FTBs. This scenario can be expected in orogenic systems bearing evaporite levels that were deposited coevally to basement faulting (this faulting being pre- or syn-contractional). However, evaporite deposition can also take place during periods of limited fault activity (such as thermal subsidence stages post-dating a rifting event) or in areas located away from the active faulting front (such as a flexural foreland basin). In this second scenario, along-strike thickness variations in the silicone décollements can be progressive. This geometrical possibility is tested systematically in the experimental program we present here. Our sets of experiments combine aspects of the aforementioned Types A and B models, such as tapered sand covers and lateral termination of décollements and are strictly focused on thin-skinned deformation scenarios.

5.2. *Experimental methodology*

5.2.1. *Analogue materials and scaling*

Experimental setups include a basal silicone layer overlain by dry sand, these two materials representing the ductile/viscous and brittle behaviour of upper crustal rocks, respectively. We used Silica Sand L-70/80 S from Sibelco Hispania that has a 99% content of quartz, a mean density of 1.610 g/cm^3 and a grain size ranging between 63 and 400 μm. Its internal friction angle (30-37°) and cohesion (40–150 Pa) were determined at the Helmholtz Laboratory for Tectonic Modelling (GFZ German Research Centre for Geosciences, Román-Berdiel et al., 2019). The selected sand behaves according to the Mohr-Coulomb criterion and shows low internal friction angles and cohesion as brittle rocks in nature do (Mandl et al., 1977; Krantz, 1991; Schellart, 2000; Panien et al., 2006; Klinkmüller et al., 2016).

To represent the ductile behaviour, the colourless silicone putty Rhodorsil Gomme FB type from Caldic was used. This silicone has a viscosity of 7×10^3 Pa s at 20 °C and a density of 0.980 g/cm^3. It has an almost perfectly Newtonian behaviour at the strain rates considered in the analogue experiments (shortening velocity of 1.5 cm/h).

Analogue models were geometrically, dynamically and kinematically scaled (Hubbert, 1937; Ramberg, 1967). We considered a length ratio of $2{\cdot}10^{-5}$, 1 cm in the models representing 0.5 km in nature (Table 2). Gravity field, viscosities and densities are imposed by the analogue materials used and the experimental conditions (see scaling ratios in Table 2). The derived, time and velocity scaling ratios (Table 2) indicate that 1 h in the experiments represents 0.14 Ma in nature whereas the shortening velocity used (1.5 cm/h) simulates a 5 mm/year shortening rate in nature.

5.2.2. *Experimental programme, set-up and procedure*

Experiments were set up over a basal mylar sheet and consisted of a basal silicone plate overlain and laterally confined by a sand package (Fig. 7). Three different sets of models were carried out: Set 1 involves constant-thickness sand and silicone layers (experiments M1a, M1b and M1c, Table 3), Sets 2 and 3 comprises experiments featuring sand and

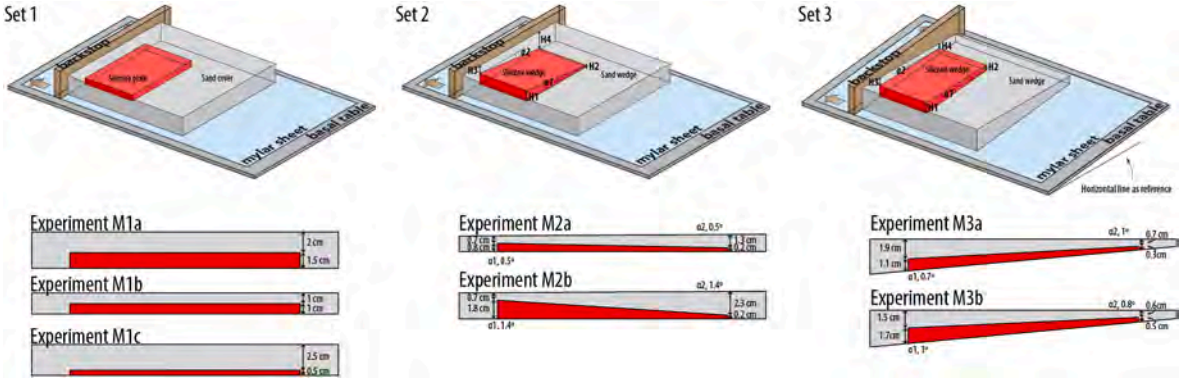

Fig. 7. Experimental set-ups used in Set 1 (left), Set 2 (centre), and Set 3 (right) experiments respectively.

Table 3
Silicone and sand thicknesses and ratios in Set 1 analogue models. *Note that M1b involves a thicker silicone layer than M1c but the total thickness is higher in M1c.

Model	Silicone (cm)	Sand cover (cm)	Total thickness (cm)	Sand/silicone ratio (cm)	Shortening (cm)
M1a	1.5	2	3.5	1.33	12
M1b	1	1	2	1	12
M1c	0.5	2.5	3	5	12

silicone layers tapered in opposite directions (Set 2, experiments M2a and M2b, Table 4) or in the same direction (Set 3, experiments M3a and M3b, Table 4). Sand and silicone thicknesses and taper angles are detailed in Tables 3 and 4 and depicted in Fig. 7. The experiments of Sets 2 and 3 had a total thickness ranging from 1.1 to 3.2 cm, with silicone/sand thickness ratios being mostly in the range of thickness ratios of Set 1 models.

All models were shortened at a constant velocity of 1.5 cm/h by pulling the basal mylar sheet from behind the rigid backstop. Total shortening was 12 cm in all experiments but M3b (total shortening, 25 cm, Table 2). A 4 or 5 cm passive grid marker recorded surface deformation. Evolution of model structures was monitored through serial photographs of the model surface, taken at regular shortening intervals of 3.75 mm. After shortening, models were wet and cut and cross-sections were photographed and structurally interpreted.

5.3. Modelling results

5.3.1. Set 1: constant-thickness sand and silicone layers

All the analogue models in this set show a notable difference between the thrust wedge detached above the central silicone plate and those developed along the lateral sand-packs bounding the silicone layer. In the sand-packs, 4 to 7 foreland-verging thrusts formed in a piggy-back thrust sequence (Fig. 8). These thrusts were closely spaced in early stages and more widely spaced during later deformation when they locally related to minor back-thrusts (e.g., Liu et al., 1992; Storti et al., 2000; Graveleau et al., 2012).

The number of structures along the silicone plate is lower than in its brittle counterpart, being limited to three main thrusts (the structure at the silicone pinch-out is here excluded). The first silicone-detached thrust emerges at the backstop and it is linear and continuous all along the silicone plate. This structure is backwards-verging (bt1 in Fig. 8A and B) in models M1a and M1b (1–1.5 cm-thick silicone, Table 2) but forwards-verging in M1c (t1 in Fig. 8C), with the thinnest silicone layer (0.5 cm). The second silicone-detached thrust (t2/bt2 in Fig. 8) forms after ~42 and 48 mm of shortening in the thinner (M1b) and thickest models (M1a and M1c), respectively. This thrust is linear and forwards-verging in the central portion of M1b, where it bends at the lateral boundaries of the silicone plate (Fig. 8). In models M1a and M1c, this thrust changes vergence along-strike (t2/bt2 in Fig. 8A and C) and predates thrust 3 (t3/bt3 in Fig. 8) that forms after ~90 and ~105 mm of shortening in the thinner (M1b) and thickest models (M1a and M1c), respectively. Its geometry varies depending on the model. It consists of (i) two relaying thrusts describing an arcuate pattern in M1a, (ii) a linear back-thrust in M1b and (iii) a relaying, discontinuous thrust displaying along-strike vergence changes in model M1c. This latter structure is partly coeval to the development of a late-shortening thrust-back-thrust pair detached along the silicone frontal pinch-out in M1c. Except t2/bt2 in model M1b, thrusts t1/bt1 and t3/bt3 emplaced synchronously or almost synchronously all along the silicone plate.

Final model geometries (Fig. 8) depict significant differences in both (i) the geometry and position of the deformation front (Fig. 8A) and (ii) the locus and extent of oblique structures. In model M1b (1 cm-thick silicone), the silicone-detached thrust system is ~11 cm-wide and the deformation front is located at a similar distance from the backstop along both the brittle and the central part of the silicone plate. In M1a and M1c, the deformation front along the silicone-detached thrust system is at a nonuniform (16–28 cm) but longer distance from the

Table 4
Silicone and sand thicknesses/ratios and taper angles tested in Set 2 and Set 4 analogue models.

Model	Silicone wedge			Sand wedge			Sand/silicone thickness ratio (cm)	Total thickness (cm)	Total Shortening (cm)
	H1 (cm)	H2 (cm)	α1 (°)	H3 (cm)	H4 (cm)	α 2 (°)			
Set 2 experiments									
M2a	0.8	0.2	0.5	0.7	1.3	0.5	0.87–6.5	1.5	12
M2b	1.8	0.2	1.4	0.7	2.3	1.4	0.39–11.5	2.5	12
Set 3 experiments									
M3a	1.1	0.3	0.7	1.9	0.7	1	1.72–2.33	3–1	12
M3b	1.7	0.5	1	1.5	0.6	0.8	0.88–1.2	3.2–1.1	25

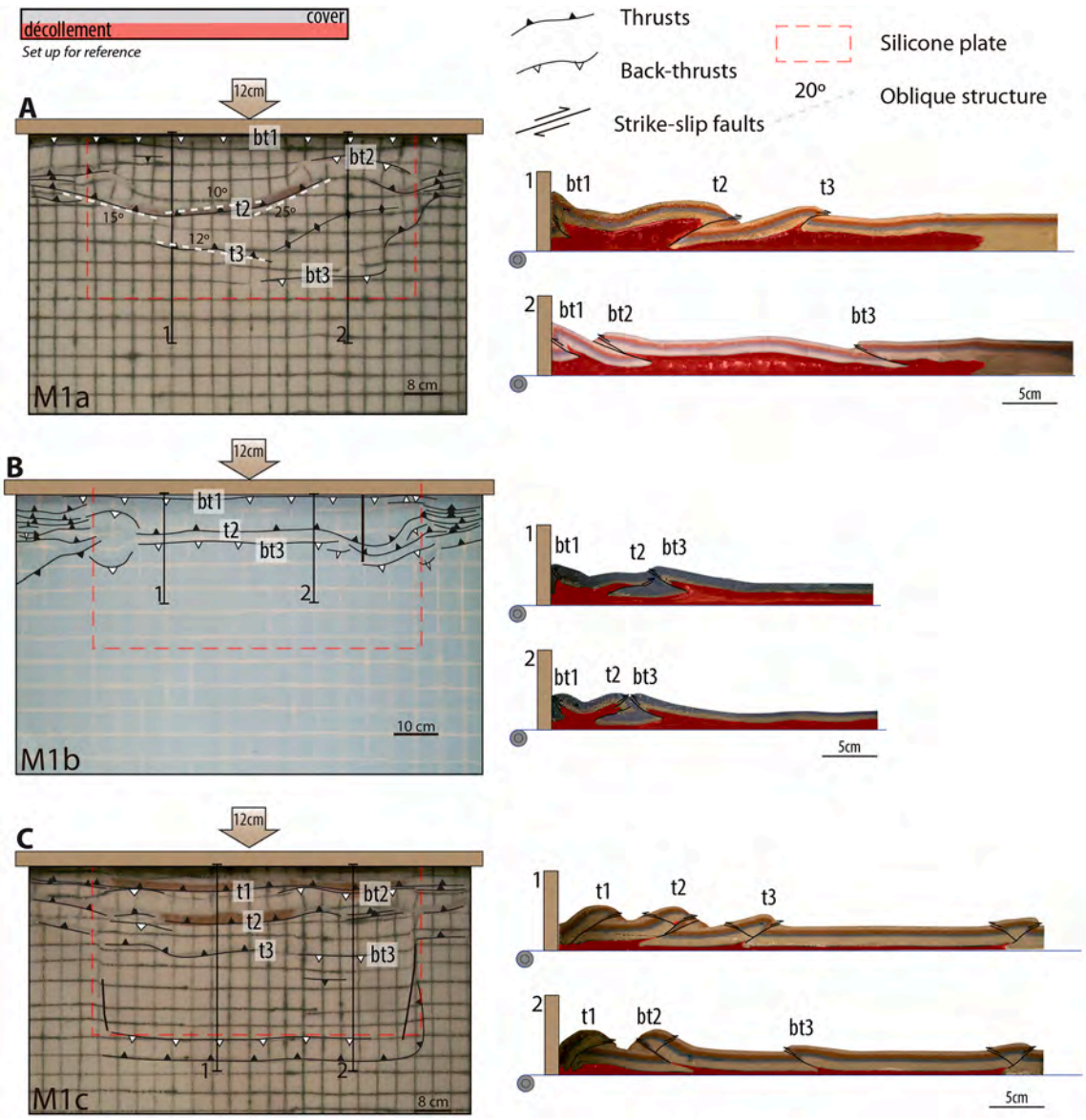

Fig. 8. Final deformation stages (top view to the left and cross section view to the right) of the three experimental models with constant-thickness sand and silicone layers. Cross section location is indicated in the top view photograph.

backstop than in the brittle model domains (13–14 cm). Regarding oblique structures, a first-order distinction can be made between M1b-M1b and M1a, where silicone thicknesses are ≤1 cm and 1.5 cm, respectively. In the first two models, obliquities are local and limited to the silicone plate boundaries (M1b) or the changing-vergence thrust segments (M1c). Conversely, in model M1a (thickest silicone), thrusts t2/bt2 and t3/bt3 are >10° oblique to the shortening direction all along their trace, describing a "regional-scale" oblique pattern.

Repetition of models M1b and M1c indicates repeatability of the main features described in this section, although vergence changes in silicone-detached thrusts t2/bt2 and t3/bt3 were not replicable. Considering all Set 1 models (including repetitions), the following general relationships can be established:

- the thrust vergence is potentially controlled by silicone thicknesses in early shortening stages (i.e., thrust t1/bt1): thinner silicone enhances forward thrusting whereas thicker silicone layers (≥1 cm in M1a-M1b) relate to early back-thrusting. Thrust vergence is nevertheless variable and non-reproducible in subsequent structures (i.e., thrusts t2/bt2 and t3/bt3), with no clear relation to silicone thicknesses and/or sand/silicone ratios.
- the width of resulting FTBs increases as the total model thickness does, independently of the thickness of the basal silicone plate or the sand/silicone ratios.
- Obliquity occurs in intermediate and late shortening structures (i.e., thrusts t2/bt2 and t3/bt3). The locus of oblique structures is controlled by silicone boundaries, lateral relays of thrusts and vergence changes with wider-scale oblique structures being exclusively developed in models with the thickest silicone (1.5 cm in M1a).

5.3.2. Set 2 and Set 3 models: along-strike thickness variations in sand/silicone layers

5.3.2.1. Set 2 experiments. Set 2 models are characterized by sand/silicone packages that taper in opposite senses (Fig. 9). Like Set 1 models, the brittle domain of Set 2 experiments is defined by 5–6 forethrusts emplaced in a piggy-back sequence. Their number decreases in the viscous domain where three major thrusts formed (Fig. 9). The first silicone-detached thrust (t1/bt1 in Fig. 9) emerges at the backstop, being

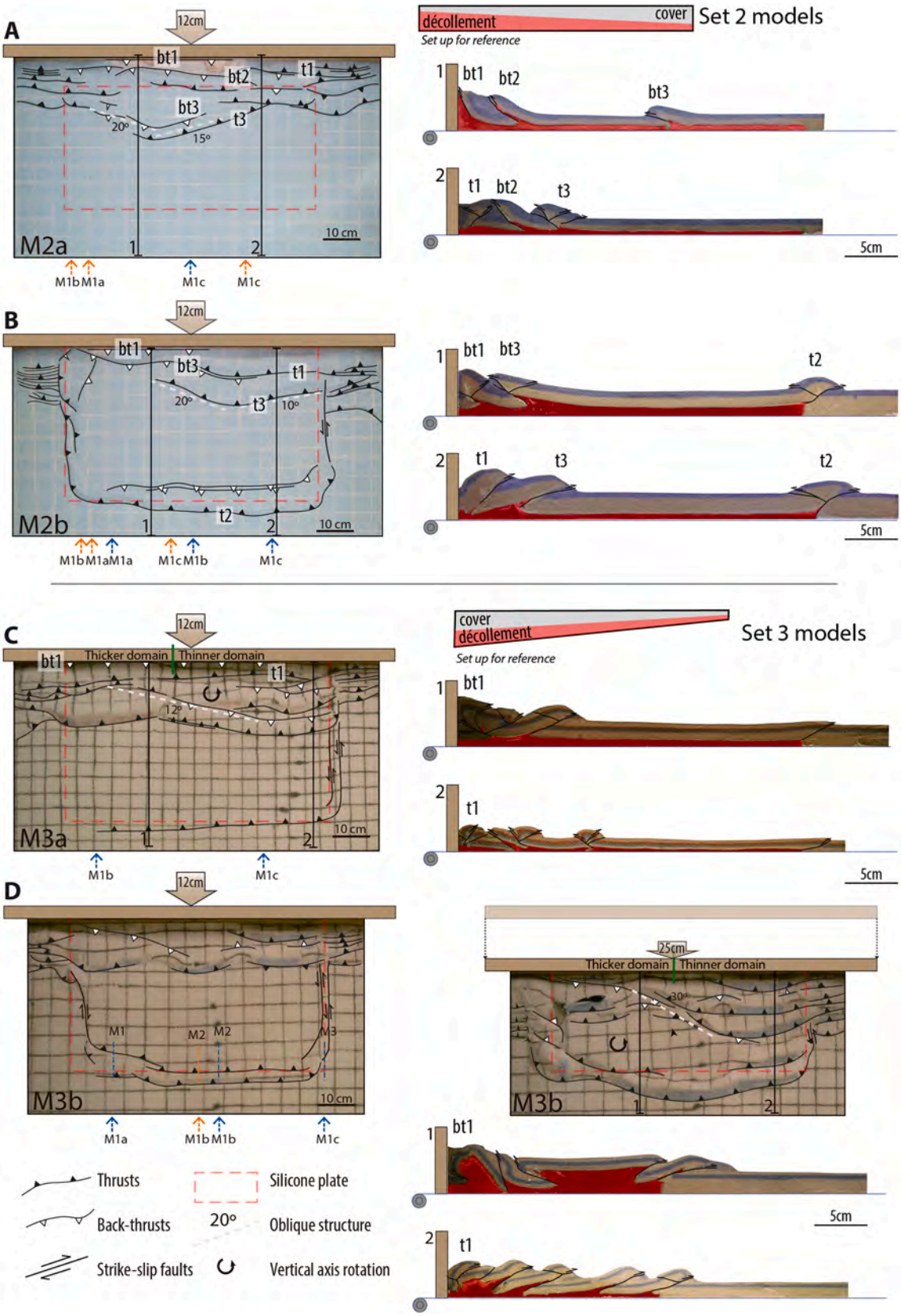

Fig. 9. Final deformation stages (top view to the left and cross section view to the right) of models M2a, M2b (Set 2 models) and M3a and M3b (Set 3 models). Cross section location is indicated in the top view photograph where oblique structures are also indicated. For model M3b, both the final deformation stage (25-cm of shortening, D, right) and the 12-cm shortening stage (D, left) are shown. Orange and blue arrows indicate the equivalent cover/décollement ratios and equivalent décollement thickness, respectively, with respect to layer-cake models of Set 1. (For interpretation of the references to colour in this figure legend, the reader is referred to the Web version of this article.)

synchronous all along the silicone plate. It is defined by a fore-directed thrust (t1) over the thinner silicone domain and its vergence changes over the thickest part of the silicone, where a main back-thrusts forms (bt1). This vergence change occurs at silicone thicknesses of ~0.4–0.5 and 1 cm in models M2a and M2b, respectively. The second silicone-detached thrust (t2/bt2 in Fig. 9) forms at the silicone pinch-out in model M2b (~4.5 cm shortening) and at a short distance from t1/bt1 in M2a. The latter changes its vergence and is diachronous along-strike: it emerges first over the thinner silicone and subsequently in the thickest silicone, at ~41 and ~75 mm of shortening, respectively. Finally, thrust t3/bt3 (out-of-sequence in M2b and in-sequence in M2a) forms also diachronously, emerging firstly over the thinner silicone and extending later on over the thickest silicone domain. It is moderately oblique to the shortening direction and consists of (i) a fore-directed thrust (thin silicone) laterally changing to a back-thrust (M2b) or (ii) two relaying thrusts describing a thrust salient (M2a, Fig. 9) and a thrust reentrant that are oblique to the regional structural trend (10–20°) and extend along-strike for 15–20 cm.

Set 2 thrust wedges are highly segmented, formed by structures that relay or curve laterally and show frequent along-strike changes of vergence (Fig. 9A and B). When only the structures detached over the inner part of the silicone are considered (i.e., structures at silicone pinch-outs are discarded), the surficial thrust front is at a shorter distance from the backstop in the thicker silicone domain in model M2b, but at a longer distance in model M2a. In M2a (smaller taper angle in the silicone, Fig. 7), although diffuse, a distinction can be made between the thrust system detached over the thinner silicone, that is doubly vergent (Fig. 9A, section 2) and the thrust system soled by the thicker silicone, which is dominated by back-thrusts (Fig. 9A, section 1). This areal distinction becomes clearer in the experiment M2b (stronger silicone taper, Table 4) where fore-directed thrusts preferentially formed over the thinner silicone whereas back-thrusts prevail over the thicker silicone (Fig. 9B).

5.3.2.2. Set 3 experiments. Set 3 models are characterized by sand/silicone packages that taper in the same direction (Fig. 7). As in Set 1 and Set 2 models, the brittle domain of Set 3 experiments is defined by a fore-directed, piggy-back thrust system. This thrust system is formed by a greater number of thrusts in the thinner, brittle domain (8 in M3a, 11 in M3b) and by a smaller number of thrusts in the thickest sand-packs (5 in M3a, 8 in M3b, note that the final shortening in M3b doubles that of M3a). This tendency in the number of structures is also identified over the silicone plate where, conversely to Set 1 and Set 2 models, the total number of structures changes laterally: thrusts are more numerous and closely spaced in the thinner part of the models but less numerous in the thicker part (Fig. 9C and D). Similarly to previously described experiments, the first silicone-detached thrust (t1/bt1in Fig. 9) is defined by a fore-directed thrust over the thinner silicone and changes its vergence over the thickest silicone where a main back-thrust forms. This vergence change occurs at silicone thicknesses of ~0.4–0.5 and 0.8–1 cm in models M3a and M3b, respectively. Subsequent silicone-detached thrusts emerge alternatingly from the thinner and thicker silicone domains and are neither continuous nor synchronous all along the silicone plate. In model M3b (Fig. 9D), a fore-directed thrust emerges at the frontal silicone pinch-out at ~2.5 cm of shortening. This thrust was long-lived and accommodated a total displacement that increased significantly from the thinner part of the model towards the thicker one.

Analogously to Set 2 experiments, thrust wedges resulting from Set 3 models consist of anastomosing thrust surfaces that relay along strike and change their geometry laterally. At final deformation stages, the surface of the models can be roughly divided into two domains (see green line in Fig. 9C and D): (1) a thinner domain, where thrusts are numerous, doubly-vergent or fore-directed and (2) a thicker doubly-vergent domain with a lower number of structures. At 12 cm shortening, the deformation front above the silicone plate (discarding the frontal structure above the silicone pinch-out) is at a similar distance from the backstop in both the thinner and thicker domains in model M3b, being at a slightly longer distance in the thinner M3a domain with respect to its thicker counterpart. Oblique structures form in the central part of the silicone wedge, in the area where thrusts from the thinner and thicker model domains converge. In model M3a, a 45-50 cm-long structure at an angle of ~12° to the regional trend can be recognized (Fig. 9C) whereas in model M3b (higher shortening, Fig. 9D), a 25 cm long oblique zone at an angle of 30° form. This structure is well-developed after 25 cm of shortening but only incipient and shorter at 12 cm of shortening (Fig. 9D). In M3b (in which we applied a higher total shortening), the thicker domain registered a small clockwise vertical axis rotation that is also identified at the thin-thick transition in model M3a after 12 cm of shortening.

5.3.3. Summary and comparison of the three sets of experiments

Although the comparison of Sets 2 and 3 models is challenging due to the simultaneous participation of several parameters, the results obtained highlight the formation of intricate thrust systems characterized by along-strike diachronous structures when tapered silicone-sand models deform. In Sets 2 and 3, silicone thicknesses play a major role on thrust vergence in earlier stages: t1/bt1 is fore-directed where the thickness of the silicone layer is below 0.4–0.5 cm and changes laterally to a back-thrust, the backwards vergence occurring always where silicone is $\geq$ 1 cm-thick. A similar relationship is observed in constant-thickness models (Set 1, section 5.3.1). Regarding the width of the resulting thrust wedge, no correlation with model thicknesses, silicone thicknesses or sand/silicone thickness ratios can be straightforwardly established in Sets 2 and 3. This relationship was nevertheless clearer in constant-thickness models (Set 1) where the thicker the model, the wider the forming thrust wedge.

Regional-scale, moderately oblique ($\leq$30°) structures occur in Sets 2 and 3. They accommodate lateral geometrical and kinematic differences along specific structures or between model domains with different silicone/sand thicknesses. In Set 3 models, obliquity increases with shortening and relates to small vertical axis rotations. When compared to constant-thickness models, regional-scale, oblique structures are only observed in model M1a, the one with the thickest silicone (1.5 cm). Existence of lateral thickness changes seems therefore to enhance the development of regional obliquities, independently of the thickness of the silicone layer.

Finally, another major difference between Set 1 and Sets 2 and 3 models relates to the timing of thrust development: in constant-thickness models, main thrusts are coeval or almost coeval along-strike whereas thrusting in analogue models with along-strike thickness variations is laterally diachronous.

6. Discussion

6.1. Experimental limitations

Summarized experiments provide numerous clues for interpreting the origin of oblique structures in FTBs. But, they also reveal the multiple controlling parameters for obliqueness, and therefore the difficulty in univocally establishing their origin. This review also highlights three main experimental limitations that should be considered when comparing previous and new models, limitations that are related to the strong heterogeneity of (i) devices, (ii) boundary conditions and (iii) materials. Even though similar materials and experimental set ups are used to perform simple plane-strain experiments, the “human factor” quantitatively conditions the results (Scheurs et al., 2006, 2016). During the past two decades, models have been performed trying to progressively reproduce settings with higher complexity. This applies especially to models involving multiple viscous décollements and/or low frictional detachments whose plain view distribution and the stratigraphic position have become particularly complicated. In general, we consider that

inferences obtained from simple models are more consistent (and generally more reproducible), although their application to particular natural examples is not as straightforward as in *ad-hoc* models. Besides, in those, the influence of a single factor may be dilute in a "sea" of different parameters tested at the same time. It must be always borne in mind, however, that resemblances between natural and analogue structures do not necessarily imply that all the variables (or variable ratios) imposed in the experimental setting are equivalent to those in nature, since different paths can often lead to similar results.

One of the difficulties in clearly defining the obliquity of structures is the intrinsic irregularity of thrust fronts developed in simple sand cake models. There, thrust fronts do not necessarily display a neat and linear trace but rather show some irregularities which tend to be homogenized by new thrusts. These obliquities are small-scale and short-lived features. Therefore, criteria for the assessment of actual oblique structures must be based on consistent patterns developed during the experiment. This can be sometimes problematic because oblique structures are often developed at the final stages of compression and some models may not reach this stage.

Regarding sand-silicone experiments, their main limitation derives from the strong rheological contrast along the sand-silicone boundary. Because of this, silicone boundaries tend to localize deformation. But such strong rheological contrast does not necessarily represent the actual properties of décollement boundaries in nature. In fact, in those areas where salt décollements gradually become less "salty", less ductile, décollement effectiveness may change progressively and the rheological contrast smooths. Latter does not apply if boundaries are related to fault planes. These limitations can be overcome using different materials with lower rheological contrasts between them (e.g., Pla et al., 2019). In centrifuge experiments, models indicate that structures showing strong obliquities with the backstop direction can develop with along-strike gradual changes in thickness in either the low-competence décollement or the overlying semi-brittle cover (Santolaria et al., 2022). Another limitation is the curvature related to boundary effects (Souloumiac et al., 2012). In addition, the push-from-behind or indentation model type has different lateral boundary conditions than the pull-from-beneath type, thus leading to different curvature effects (Scheurs et al., 2006). Such effect can be reduced by lubricating the boundary between the analogue materials and the sidewalls (e.g., Costa and Vendeville, 2002; Santolaria et al., 2015).

6.2. *Understanding oblique structures from analogue modelling*

Analogue models analysing the influence of along-strike thickness and rheology changes show that it is not necessary an a priori irregular geometry of the backstop (indenter, corner-shaped, etc …; Fig. 1A–D) to produce oblique structures in a purely frictional cover (no décollement involved). When thickness changes are progressive, oblique structures develop and extend along-strike as much as the thickness change does. Their obliquity with regard to the rectilinear backstops (Soto et al., 2003) attains 10-15° when considering doubly-vergent wedges, increasing to more than 30° in the case of mono-vergent wedges (Soto et al., 2002). In doubly vergent wedges, obliquity also involves the retro-wedge (i.e., strike changes distributed between the pro- and the retro-wedge). When thickness changes in the sand pack are sharper, oblique structures are generally limited to a few centimetres wide domain along the area where the thickness change is located. Angles with respect to the backstop are generally higher than in the models displaying progressive thickness variations, being commonly close or larger than 45°. All in all, obliquity is strictly related to the geometry, especially the width of the sand wedges: the thicker the sand pack, the wider the thrust systems whereas the thinner the sand pack, the narrower the thrust systems. Thrusts are more abundant in the thinner domains of the experiments where individual structures accommodate displacements that are more limited than in the thrusts developed in adjacent thicker domains. Apart from the lateral variations in thrust geometries, models exploring lateral thickness changes in a brittle cover shed light on wider-scale processes such as piggyback basin formation and evolution in orogens (Leturmy et al., 2000) or tectonic topography evolution due to thrusting (Chauhan et al., 2009). These models can be applied to orogens where pre-contractional, lateral thickness variations derive from a previous stage of differential, along-strike lithospheric/crustal stretching (e.g. Pyrenees, Jammes et al., 2010; 2014; Tugend et al., 2014) or from previous stages of basin formation in the upper crust (e.g. Southern Andes, Likerman et al., 2013).

Backstop thickness and geometry changes also offer a promising field for explaining a variety of oblique structures developed in FTBs (Marshak et al., 1992; Lu et al., 1998; Macedo and Marshak, 1999). Both gradual and sharp thickness changes have been proposed, resulting in the formation of oblique structures nucleated in these irregularities. Obliquity strongly depends on the shape of the tested backstop and can reach 90° when backstop thickness changes are sharp (Fig. 3C, D, E, F; Macedo and Marshak, 1999) although limited obliquities (10-15°) are attained when using tapered backstops (Fig. 5c; Soto et al., 2006b).

Sand-silicone systems are more difficult to systematize because, as previously mentioned, the geometrical possibilities of décollement distribution are even higher than those of the backstop geometries, and new models imposing different boundary conditions are being continuously developed. Common features in these models include the formation of structures along the silicone plate boundaries, either parallel or oblique to them. Silicone boundaries that run subparallel to the shortening direction generally promote the development of oblique structures at moderate to high angles to the backstop. In some experiments, this behaviour induces the occurrence of strike-slip or transfer faults along silicone boundaries and the linkage of different thrust fronts (Fig. 4). The rapid transference of deformation from near-to-the-backstop areas to the distal pinch-out boundary of silicone plates is also a common feature in most of the models and must be considered when applying results from models to nature.

The joined effect of thickness variations in the brittle cover and the presence of viscous décollements (Storti et al., 2007, Fig. 5d; this study; Figs. 8 and 9) prompts thrust geometries that combine features from the two previous, individual parameters. On the one hand, silicone boundaries usually localize deformation, this localization being stronger when the angle of overlying sand wedges is higher (models M2b, M3a and M3b in Fig. 9), independently on the thickness of the underlying silicone. In constant-thickness models, development of structures at silicone boundaries seems less frequent (models M1a to M1c in Fig. 8) which suggests that this effect can be enhanced by thickness variations in cover packages overlying viscous décollements. On the other hand, the varying thickness of the cover produces thrust systems that are much more segmented than in sand-silicone models where viscous layers are overlain by a constant thickness sand pack (compare models in Figs. 8 and 9). Oblique structures frequently develop over the inner part of the silicone plate (not only in their boundaries). The comparison between previous and new models emphasizes that, independently of the thickness of the viscous décollement, along-strike, décollement/cover thickness variations, can trigger regional-scale oblique structures running at moderate angles ($\leq$30°) to the backstop. Obliquity is enhanced by increasing shortening and oblique features accommodate lateral changes in the vergence or number of structures that are controlled by the total thickness of the sand-silicone package and the sand-silicone thickness ratio.

7. Comparison with natural examples

Natural prototypes that inspired the revised series of analogue models involve processes at different scales framed on the upper crust (foreland basins, FTBs, orogens and accretionary complexes) and the lower crust and the asthenosphere (continental collision), including i) FTBs in the Himalayas (Marshak et al., 1992; Macedo and Marshak, 1999; Cotton and Koyi, 2000; Smit et al., 2003; Storti et al., 2007; Li and

Mitra, 2017), Tibet (Calassou et al., 1993; Marques and Cobbold, 2002; Sun et al., 2016), Kuqa basin in the Southern Tian Shan (Li and Mitra, 2017; Borderie et al., 2018), Verkhoyansk Range in Siberia (Marshak et al., 1992; Macedo and Marshak, 1999), Zagros Mountains (Macedo and Marshak, 1999; Storti et al., 2007; Bahroudi and Koyi, 2003; Callot et al., 2012; Farzipour-Saein and Koyi, 2014), Pindos in Greece (Bigi et al., 2009), Carpathians (Marshak et al., 1992; Macedo and Marshak, 1999), Alps (Calassou et al., 1993; Philippe et al., 1998; Macedo and Marshak, 1999; Lickorish et al., 2002; Ravaglia et al., 2006), Jura Mountains (Macedo and Marshak, 1999; Smit et al., 2003; Li and Mitra, 2017), Apennines (Corrado et al., 1998; Macedo and Marshak, 1999; Bonini, 2007; Bigi et al., 2009), Southern Pyrenees (Soto et al., 2002, Sans, 2003; Koyi and Sans, 2006; Soto et al., 2006b; Storti et al., 2007; Bigi et al., 2009; Vidal-Royo et al., 2009; Santolaria et al., 2015; Van der Werf et al., 2023), Gibraltar Arc (Luján et al., 2003), Espinhaço thrust belt in Brazil (Marshak and Wilkerson, 1992), Central Andes (Marques and Cobbold, 2002), Urica fault zone in Venezuela (Calassou et al., 1993), West Spitsbergen in Greenland (Bigi et al., 2009), the Betic Cordillera (Ter Borgh et al., 2011) and the Western Taiwan Thrust Wedge (Lu et al., 1998) and ii) accretionary complexes in Lesser Antilles Volcanic Arc in the Caribbean plate (Calassou et al., 1993; Soto et al., 2003), and the Manila accretionary system (Soto et al., 2003). In the following sections, we compare to the analogue models two salt-detached case studies featuring thrust salients of different scales and highly (South Pyrenean Central Salient) to moderately oblique (Keping Shan FTB) structures. Apart from these examples, our experimental results may also help understand some of the aforementioned FTBs used as natural prototypes by previous authors.

7.1. Comparison with the South Pyrenean Central Salient

The South Pyrenean Central Salient (SPCS), located in the Southern Pyrenees, provides one of the most interesting and better studied examples of thrust salient (Sussman et al., 2004; Muñoz et al., 2013). It displays a south-verging curved shaped in map view (Fig. 10A) where central structures trend parallel to the chain (~N120E) while lateral structures strike highly oblique to it. This thrust salient consists of three fore-directed thrust sheets (Fig. 10A and B) emplaced between the

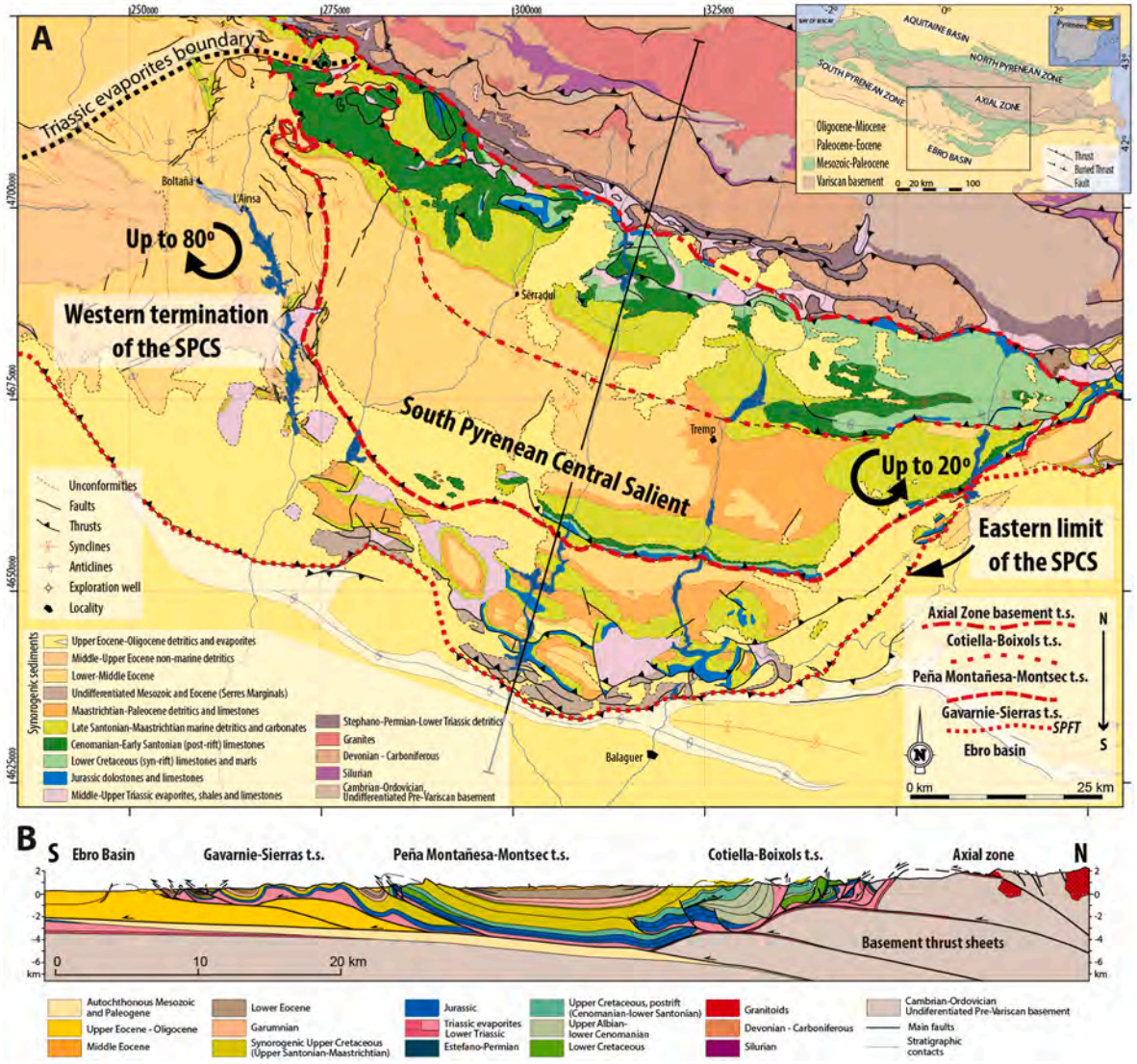

Fig. 10. A) Synthetized geological map of the South-Central Pyrenees where main thrust sheets of the South Pyrenean Central salient are displayed (see top-right corner for regional location). Note their curved shape as well as the orientation of central to lateral structures. Vertical axis rotations, indicated by black circle arrows are also shown. Modified after Muñoz et al. (2013, 2018), Clariana et al. (2022) and Soto et al. (2022). B) Geological cross-section across the central part of the South Pyrenean Central Salient (modified from Teixell and Muñoz (2000) according to García-Senz (2002), Muñoz et al. (2018)). Black straight line as the section trace line in Fig. 10A.

Cretaceous and the Oligocene, mainly following a forward propagating sequence (e.g. Muñoz, 1992; Beaumont et al., 2000). These thrust sheets detached over Triassic evaporites, the regional décollement of the Pyrenees.

The syn-, post-rift and syn-contractional Mesozoic succession in the SPCS thins southwards, from up to 5000 m in the northernmost thrust sheet to less than 300 m in the south Pyrenean front. An east to west, smoother, along-strike thinning also occurs (Soto et al., 2002, 2003). In its turn, the Triassic décollement pinches out towards the eastern and western edges of the salient (see limit of the Triassic décollement in Fig. 10). In the eastern boundary, South Pyrenean units thrust over the Ebro Basin defining a neat limit of the salient, the oblique structures occupy a relatively narrow area close to the limit (10–15 km wide) and they underwent slight (~20°) counter-clockwise vertical axis rotations (Dinarès et al., 1992; Sussman et al., 2004). On the contrary, the western limit is diffuse, obliquity of structures is higher and distributed along a wider area (40–50 km). Paleomagnetism reveals that these structures were emplaced with a subtle obliquity (Mochales et al., 2012; Muñoz et al., 2013) and then they underwent a high (up to 80°) clockwise vertical axis rotation (Bentham, 1992; Fernández et al., 2003; Sussman et al., 2004; Mochales et al., 2012; Muñoz et al., 2013) during Eocene-Oligocene times. Accordingly, this salient has been classified as a progressive arc (Sussman et al., 2004; Muñoz et al., 2013).

All in all, this salient is characterized by i) pre-contractional basin-related geometries such as along and across strike thickness variations in the décollement and the overlying sedimentary sequence, that partly promote, during mountain building, ii) a variable structural wavelength, occurrence of oblique structures and its characteristic salient geometry. These features makes this natural example comparable to the following experimental programs:

i) those set-ups including a tapered brittle cover as in Soto et al. (2002, 2003 and 2006b) and Bigi et al. (2009) or Storti et al. (2007) who, in addition, included a basal viscous décollement that ends laterally and forelandwards. Those features may simulate the Mesozoic basin architecture of the salient.
ii) by Lickorish et al. (2002), Izquierdo-Llavall and Casas Sainz (2012), Van der Werf et al. (2023) and our new experimental program. These set ups include a tapered cover on top of a tapered salt-analogue décollement, features that may converge in the SPCS.
iii) since the basement thrusts (Axial Zone, in Fig. 10A and B) driving the deformation in the supra-detachment cover are not linear and do not show a homogeneous and synchronous displacement along the chain, a curved backstop (Jiménez-Bonilla et al., 2020 and references therein) could also be accounted for some of the rotational features, regardless of the thickness changes in the cover.

Lateral thickness variations in sand pack models (Soto et al., 2002, 2003, 2006b) triggered, from the thick domain to the thin one, a much more advanced thrust front that laterally transitions to a retreated front where structural wavelength decreases (Fig. 5A). This thrust front is emplaced slightly obliquely to the strike of the moving wall. These observations give analogue-based arguments that support the oblique emplacement hypothesis (prior to vertical axis rotation, Mochales et al., 2012; Muñoz et al., 2013) of folds in the western edge of the SPCS.

When considering a salt-analogue décollement, its distribution becomes a major controlling factor of deformation. As mentioned, a symmetrical, along-strike tapering of the décollement-cover sequence (Lickorish et al., 2002) leads to a symmetrical, slightly curved FTB whose geometry does not fully fit with the asymmetry of the SPCS. Therefore, a different décollement-cover geometry is needed. In those experiments where basal décollements pinch out laterally, transfer zones and oblique structures form along the rheological discontinuity and tend to mimic the distribution of the décollement. This is not the case if an along-strike tapered cover lies on top of a constant thickness décollement (Storti et al., 2007). In this case, thrust wedge grows asymmetrically and depict transpressional faulting where the cover is thicker and curved structures which register vertical axis rotations towards the opposite side, where the cover is thinner. Despite the asymmetry obtained in these models, the relatively sharp limits of the analogue salient do not entirely fit with the ones observed in the SPCS, whose western limit is more diffuse. This points to a gradual thinning of the Triassic evaporites (and its overlying cover) rather than to an abrupt termination of them. Our models and those by Van der Werf et al. (2023) contemplate a scenario (experiments M3a and M3b, Figs. 7 and 9) in which counterclockwise vertical axis rotation occurred along the thinner décollement cover domain. Still despite the thin décollement, a transfer zone formed along the rheological contrast found in its pinch-out. Besides, in our models, oblique structures were found in the central area of the experiments, features that are not observed in the SPCS. Regarding our models, the influence that the thickness of the salt has on the vergence of structures hampers a direct comparison with the SPCS.

Some of the tested parameters and analogue results indicate that the formation of the SPCS likely responds to multiple factors. Yet, none of the experimental programs achieved a completely satisfactory simulation of such salient, especially regarding its western termination where highly oblique structures occurred along a tens of kilometres-wide area. A different set-up configuration may be needed (Muñoz et al., this volume).

7.2. Comparison with the Keping Shan fold-and-thrust system (NW China)

The Keping Shan, in NW China, is an active FTB resulting from the far-field effects of the collision between the Indian subcontinent and the Eurasian plate (Molnar and Tapponnier, 1975; Avouac et al., 1993; Replumaz and Tapponnier, 2003). From the Eocene to the present, this plate collision produced intraplate deformation and strong vertical uplift in the Tian Shan Range (Coleman, 1989).

The Keping Shan FTB forms a long and arcuate thrust salient described as an imbricate and dominantly south-verging system formed during late Cenozoic times (Allen et al., 1999, Fig. 11A). Its geometry is dominated by thrusts and related fault-bend folds (Fig. 11B).

The Keping Shan FTB is inferred to detach along a thin layer of Upper Cambrian salt (Allen et al., 1999) which does not crop but in the northwest of the Tarim basin (Lin et al., 1992). There, they consist of a few tens of meters-thick sequence, affected by dissolution and brecciation (Allen et al., 1999). Overlying the detachment, an Upper Cambrian to Permian sequence is overlain by Neogene detrital units (Turner et al., 2010, Fig. 11). Palaeozoic sequence displays a general thickening to the East, mostly related to thickness changes in the Permian succession (Turner et al., 2010, 2011, Fig. 11C). These thickness variations are associated with a series of inherited, Permian in age, NNW-SSE-striking basement faults subsequently reactivated during the late Cenozoic compression (Turner et al., 2011).

The Dabantagh fault zone (see location in Fig. 11A) is one of these inherited structures: it represents the transition between an eastern domain, characterized by a thicker (5–7 km) Cambrian-Permian sequence, and a western domain where Cambrian to Permian units are thinner (3–4 km) and more strongly compartmentalized by oblique basement features (such as the Piqiang Fault, Fig. 11A, C). When the Dabantagh fault zone is considered, the Keping Shan FTB can be divided into (1) an eastern area, where thrusts strike NE-SW, subparallel to the regional trend in the Tian Shan and (2) a western domain where thrusts bend along-strike to become slightly oblique to the frontalmost structure in the Tian Shan (the South Tian Shan fault, Fig. 11). Thrusts are frequently interrupted by strike slip faults and lateral and oblique thrust ramps. The eastern area (thicker Palaeozoic sequence) features less and widely-spaced thrusts whereas in the western domain (thinner Palaeozoic sequence), thrusts are more abundant and narrower. Besides, the

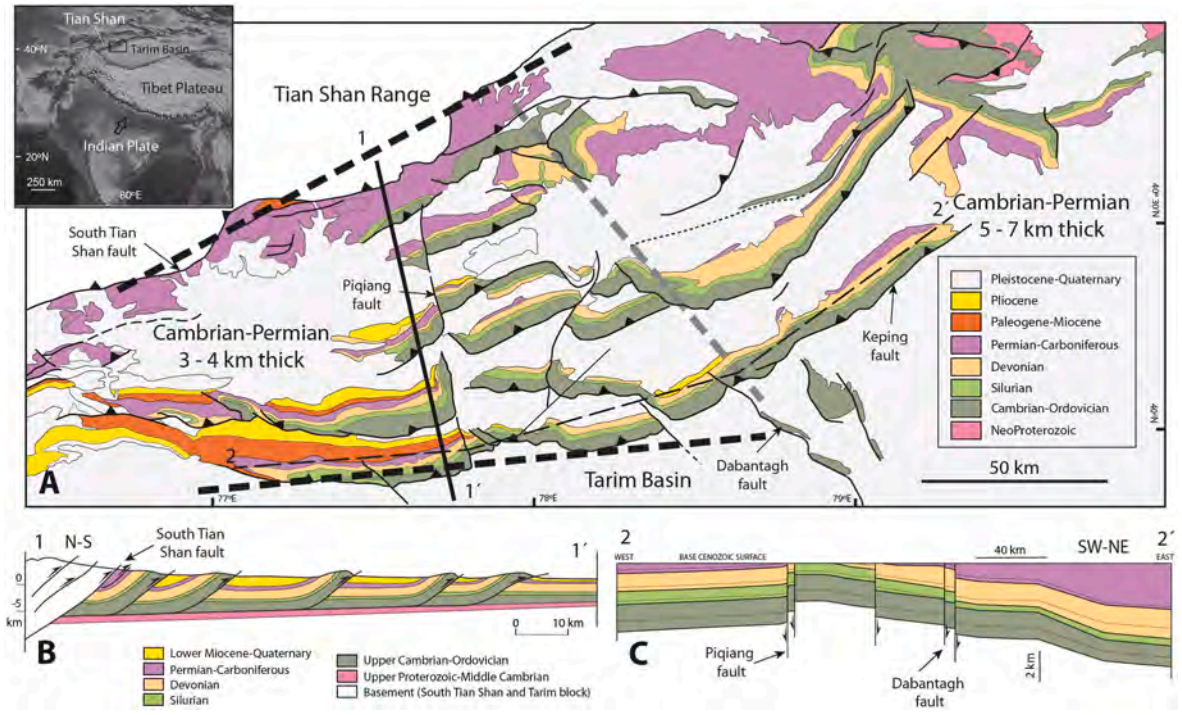

Fig. 11. A) Geological map of the Keping Shan fold-and-thrust belt (modified from Turner et al., 2010). See top-left corner for regional location. To the North, the South Tian Shan fault marks the transition between the southern Tian Shan Range and the Keping Shan fold-and-thrust belt that affects the northern part of the Tarim foreland basin. Approximate thicknesses of the Cambrian-Permian sequences deformed by the thrust system are indicated. B) Geological cross-section across the western part of the Keping Shan fold-and-thrust system (redrawn from Allen et al., 1999). See location in Fig. 11A. C) Stratigraphic correlation panel built from stratigraphic sections along the hangingwall of the Keping fault (redrawn from Turner et al., 2010). See location in Fig. 11A. Note thickness variations in the Cambrian-Permian sequence across the Piqiang and Dabantagh faults.

frontalmost structure in the Keping Shan defines an outer envelope that strikes roughly oblique (~20-25°) to the south Tian Shan structural trend.

The laterally changing number of thrusts in the Keping Shan FTB has been proposed to result from lateral changes in the thickness of the Palaeozoic units involved (Turner et al., 2010, 2011) as observed in analogue models featuring along-strike thickness changes (either sharp or progressive; Calassou et al., 1993; Soto et al., 2002). Reviewed models (Calassou et al., 1993; Macedo and Marshak, 1999; Philippe et al., 1998; Soto et al., 2002; Soto et al., 2003; Storti et al., 2007; see Fig. 2A, G, 2M, 2H, 2I, 3A; for comparison purposes, the South Tian Shan fault can be considered analogous to an experimental rigid backstop) indicates that also the geometry of the outer envelope of the Keping Shan thrust system is likely controlled by the westwards, general thickness decrease of the deformed stratigraphic sequence. Comparison of our analogue models and previous studies (Storti et al., 2007) show that, in salt-detached thrust systems as the Keping Shan, such regional obliquities are enhanced by constant-thickness viscous décollements overlain by a shallow along-strike sand taper. Tapered viscous décollements (Van der Werf et al., 2023; this study) also promote the development of regional obliquities in the range of those observed in the Keping Shan FTB. They nevertheless tend to relate to deformation fronts that are more advanced in the model domains where the brittle cover is thinner (except in experiment M2b). Analogue modelling results (Storti et al., 2007; this study) also indicate that along-strike diachronous thrusting in the Keping Shan can result from along-strike thickness variations in the deformed sedimentary sequence.

To the East and to the West of the Keping Shan FTB, the Tarim Basin is formed by a Mesozoic-Cenozoic sequence which is thicker than in the Keping FTB (up to 10 km, Allen et al., 1999). Thrusts in these areas emerge at a shorter distance from the South Tian Shan fault than the folds and thrusts in the thin-skinned Keping Shan FTB. The Keping Shan FTB therefore depicts a thrust salient geometry which likely relates to (i) the lateral termination of regional décollements East and West of it or (ii) the thick Meso-Cenozoic units in the Tarim domains bounding the Keping Shan FTB, which could suppress the ability of regional décollements to propagate deformation further into the foreland (Allen et al., 1999). These geometries, resulting from sharp thickness changes in the deforming sedimentary pile, agree with those obtained in the analogue models by Corrado et al. (1998) where thicker sand packages correlate to narrower, thick-skinned thrust systems whereas thinner sand packages (involving an interbedded viscous décollement) yield the formation of wider, thin-skinned thrusts systems that propagate at longer distances from the backstop (Fig. 6C).

8. Conclusions

The origin and evolution of oblique structures in thrust wedges have been widely studied by experimental analogue modelling. One of the main factors favouring the creation of oblique structures is the along-strike thickness variation of the deforming analogue stratigraphy. With this purpose, analogue modellers tested this factor by means of irregular or tilted basal plates, shaped backstops, sharp or gradual changes in the topography at the top of the models, which means abrupt or progressive thinning trends, and cover/décollement thickness ratio changes. In this work, we have compiled and described previous experimental programs and analogue results and completed them with sets of new models featuring, simultaneously, a tapered cover and underlying décollement. Results are interpreted in the light of three baseline, constant-thickness models where sand/silicone ratios are comparable to those considered in tapered experiments.

From the overall dataset (previous and new models), main experimental trends are described and analysed. In sand packs, sharp cover thickness offsets (parallel or oblique to the shortening direction), result in a wider thrust wedge over the thicker model domain and a narrower thrust wedge over the thinner one. Between domains, deformation is

constrained into a transfer zone where oblique structures develop. This abrupt transition is not observed when considering gradually tapered sand packs where the outer envelope of the deformed state is gradual and oblique to both the shortening direction and the strike of the backstop.

Analogue modelers have considered a wide range of basal and/or interlayered viscous-ductile décollement geometries in horizontally topped sand packs. Experiments depict curved shapes, transfer zones along the décollement pinch-outs, vertical axis rotations and out-of-sequence thrusting. When tapered sand covers are considered together with tapered or constant thickness décollements, thrust systems within viscous domains are asymmetric, formed by structures with variable length, along-strike changes in vergence and curved geometries in plan-view. More specifically, the new models presented in this study highlight that along-strike, tapered viscous systems are characterized by along-strike diachronous structures, with décollement thicknesses controlling thrust vergence in earlier shortening stages. Tested set-ups show the development of moderately oblique ($\leq 30^{\circ}$) structures that accommodate geometrical and kinematic differences along particular structures or between model domains with different silicone/sand thicknesses.

Investigated series of models were compared with a broad range of natural examples. We have revisited two particular thrust systems: the South Pyrenean Central Salient, and the Keping Shan FTB. These are detached over viscous, evaporitic décollements that favour the development of thrust salients of different scales and oblique structures. Their décollements end and change thickness laterally and are overlain by sedimentary sequences that display along-strike thickness variations. The distribution and extent of oblique structures, the lateral variation in the number, width and vergence of the main folds and thrusts and the location of salt-structures in the natural case studies could be partly predicted from the known cover/décollement thickness variations and the results of the analogue models summarized/presented in this work.

CRediT authorship contribution statement

Pablo Santolaria: Conceptualization, Investigation, Methodology, Writing – original draft, Writing – review & editing. **Esther Izquierdo-Llavall:** Conceptualization, Formal analysis, Investigation, Methodology, Writing – original draft, Writing – review & editing. **Ruth Soto:** Conceptualization, Investigation, Methodology, Writing – original draft, Writing – review & editing. **Teresa Román-Berdiel:** Conceptualization, Investigation, Methodology, Writing – original draft, Writing – review & editing. **Antonio Casas-Sainz:** Conceptualization, Investigation, Methodology, Writing – original draft, Writing – review & editing.

Declaration of competing interest

The authors declare the following financial interests/personal relationships which may be considered as potential competing interests: Antonio Casas-Sainz reports financial support was provided by Ministerio de Ciencia e Innovación (Gobierno de España). Teresa Roman-Berdiel reports financial support was provided by Ministerio de Ciencia e Innovación (Gobierno de España). Ruth Soto reports financial support was provided by Ministerio de Ciencia e Innovación (Gobierno de España).

Data availability

Data will be made available on request.

Acknowledgements

The authors are grateful to Marco Bonini and Oskar Vidal for his comments to an earlier version of the manuscript, and to two anonymous reviewers and Mark Rowan and Sandra Borderie, as editors, for their helpful suggestions to the current version. This work is part of the I+D+i research projects CGL2016-77560-C2, PID2019-108753 GB-C2 and PID2020-114273 GB-C22 funded by MICIN/AEI/10.13039/501100011033 and by "ERDF A way of making Europe".

References

Allen, M.B., Vincent, S.J., Wheeler, P.J., 1999. Late Cenozoic tectonics of the Kepingtage thrust zone: interactions of the tien Shan and Tarim Basin, northwest China. Tectonics 18 (4), 639–654.

Avouac, J.P., Tapponnier, P., Bai, M., You, H., Wang, G., 1993. Active thrusting and folding along the northern Tien Shan and late Cenozoic rotation of the Tarim relative to Dzungaria and Kazakhstan. J. Geophys. Res. Solid Earth 98 (B4), 6755–6804.

Baars, D.L., See, P.D., 1968. Pre-Pennsylvania stratigraphy and paleotectonics of the san juan mountains, southwestern Colorado. Geol. Soc. Am. Bull. 79, 333–349.

Bahroudi, A., Koyi, H.A., 2003. Effect of spatial distribution of Hormuz salt on deformation style in the Zagros fold and thrust belt: an analogue modelling approach. J. Geol. Soc. 160, 719–733.

Bahroudi, A., Koyi, H.A., Talbot, C.J., 2003. Effect of ductile and frictional décollements on style of extension. J. Struct. Geol. 25 (9), 1401–1423.

Beaumont, C., Muñoz, J.A., Hamilton, J., Fullsack, P., 2000. Factors controlling the Alpine evolution of central Pyrenees inferred from a comparison of observations and geodynamical models. J. Geophys. Res. Solid Earth 105 (B4), 8121–8145. https://doi.org/10.1029/1999JB900390.

Bentham, P., 1992. The Tectono-Stratigraphic Development of the Western Oblique Ramp of the South-Central Pyrenean Thrust System, Northern Spain. Tesis doctoral, Univ. de Southern California, p. 253.

Bigi, S., Galuppo, C., Perfetti, L., Colella, S., Civalleri, M., 2009. Along-strike pre-orogenic thickness variation and onlapping geometries control on thrust wedge evolution: insights from sandbox analogue modelling. Trab. Geol. 29, 119–128.

Bonini, M., 2007. Deformation patterns and structural vergence in brittle-ductile thrust wedges: an additional analogue modelling perspective. J. Struct. Geol. 29, 141–158.

Borderie, S., Gravelaeau, F., Witt, C., Vendeville, B.C., 2018. Impact of an interbedded viscous décollement on the structural and kinematic coupling in fold-and-thrust belts: insights from analogue modeling. Tectonophysics 722, 118–137.

Bosboom, R., Dupont-Nivet, G., Huang, W., Yang, W., Guo, Z., 2014. Oligocene clockwise rotations along the eastern Pamir: tectonic and paleogeographic implications. Tectonics 33 (2), 53–66.

Calassou, S., Larroque, C., Malavieille, J., 1993. Transfer zones of deformation in thrust wedges: an experimental study. Tectonophysics 221, 325–344.

Callot, J.P., Trocmé, V., Letouzey, J., Albouy, E., Jahani, S., Sherkati, S., 2012. Preexisting salt structures and the folding of the Zagros Mountains. In: Alsop, G.I., Archer, S.G., Hartley, A.J., Grant, N.T., Hodgkinson, R. (Eds.), Salt Tectonics, Sediments and Prospectivity, vol. 363. Geological Society, London, pp. 545–561. Special Publications. https://doi.org/10.1144/SP363.27.

Capote, R., Muñoz, J.A., Simón, J.L., Liesa, C.L., Arlegui, L.E., 2002. Alpine tectonics I: the Alpine system north of the betic cordillera. In: Gibbons, W., Moreno, T. (Eds.), The Geology of Spain. The Geological Society, London, pp. 367–400.

Casas, A.M., Cortés, A.L., Gapais, D., Nalpas, T., Román, T., 1998. Modelización analógica de estructuras asociadas a compresión oblicua y transpresión. Ejemplos del NE peninsular. Rev. Soc. Geol. Espana 11 (3–4), 331–344.

Cerca, M., Ferrari, L., Bonini, M., Corti, G., Manetti, P., 2004. The role of crustal heterogeneity on controlling vertical coupling in a transform plate boundary: analogue modelling and comparison with Early Tertiary deformation in southern Mexico. In: Grocott, J., Taylor, G., Tikoff, B. (Eds.), Vertical Coupling and Decoupling in the Lithosphere, vol. 227. Geological Society, London, Special Publication, pp. 117–140.

Chattopadhyay, A., Jain, M., Bhattacharjee, D., 2014. Three-dimensional geometry of thrust surfaces and the origin of sinuous thrust traces in orogenic belts: insights from scaled sandbox experiments. J. Struct. Geol. 69, 122–137.

Chauhan, A.P.S., Singh, S.C., Hananto, N.D., Carton, H., Klingelhoefer, F., Dessa, J.-X., Permana, H., White, N.J., Graindorge, D., SumatraOBS Scientific Team, 2009. Seismic imaging of forearc backthrusts at northern Sumatra subduction zone. Geophys. J. Int. 179, 1772–1780.

Cifelli, F., Caricchi, C., Mattei, M., 2016. Formation of arc-shaped orogenic belts in the Western and Central Mediterranean: a palaeomagnetic review. Geological Society, London, Special Publications 425, SP425, 12.

Clariana, P., Soto, R., Ayala, C., Casas-Sainz, A.M., Román-Berdiel, T., Oliva-Urcia, B., et al., 2022. Basement and cover architecture in the Central Pyrenees constrained by gravimetric data. Int. J. Earth Sci. 111, 641–658.

Coleman, R.G., 1989. Continental growth of northwest China. Tectonics 8 (3), 621–635.

Corrado, S., Di Bucci, D., Naso, G., Faccenna, C., 1998. Influence of palaeogeography on thrust system geometries: an analogue modelling approach for the Abruzzi-Molise (Italy) case history. Tectonophysics 296, 437–453.

Costa, E., Vendeville, B.C., 2002. Experimental insights on the geometry and kinematics of fold-and-thrust belts above weak, viscous evaporitic décollement. J. Struct. Geol. 24, 1729–1739.

Cotton, J.T., Koyi, H.A., 2000. Modeling of thrust fronts above ductile and frictional detachments: application to structures in the Salt Range and Potwar Plateau, Pakistan. GSA Bulletin 112 (3), 351–363.

Craddock, J.P., Kopania, A.A., Wiltschko, D.W., 1988. Interaction between the Northern Idaho-Wyoming thrust belt and bounding basement blocks, Central Western Wyoming. Geol. Soc. Am. Mem. 171, 333–352.

Crespo-Blanc, A., 2008. Recess drawn by the internal zone outer boundary and oblique structures in the paleomargin-derived units (Subbetic Domain, central Betics): an analogue modelling approach. J. Struct. Geol. 30 (1), 65–80.
Crespo Blanc, A., González Sánchez, A., 2005. Influence of indenter geometry on arcuate fold-and-thrust wedge: preliminary results of analogue modelling. Geogaceta 37, 11–14.
Crespo-Blanc, A., Comas, M., Balanyá, J.C., 2016. Clues for a Tortonian reconstruction of the Gibraltar Arc: structural pattern, deformation diachronism and block rotations. Tectonophysics 683, 308–324.
Crespo-Blanc, A., Jiménez-Bonilla, A., Balanyá, J.C., Expósito, I., Díaz-Azpiroz, M., 2017. Influence of diapirs on the development of non-cylindrical arcuate fold-and-thrust belts: results from analogue models of progressive arcs. Geogaceta 61.
Dahlstrom, C.D.A., 1970. Structural geology in the eastern margin of the Canadian Rocky Mountains. Bull. Can. Petrol. Geol. 18, 332–406.
Davis, D.M., Engelder, T., 1985. The role of salt in fold-and-thrust belts. Tectonophysics 119 (1–4), 67–88.
Dinarès, J., McClelland, E., Santanach, P., 1992. Contrasting rotations within thrust sheets and kinematics of thrust tectonics as derived from palaeomagnetic data: an example from the Southern Pyrenees. In: Thrust Tectonics. Springer Netherlands, pp. 265–275.
Dooley, T.P., Hudec, M.R., 2020. Extension and inversion of salt-bearing rift systems. Solid Earth 11, 1187–1204. https://doi.org/10.5194/se-11-1187-2020.
Duffy, O.B., Dooley, T.P., Hudec, M.R., Jackson, M.P.A., Fernandez, N., Jackson, C.A.L., Soto, J.I., 2018. Structural evolution of salt-influenced fold-and-thrust belts: a synthesis and new insights from basins containing isolated salt diapirs. J. Struct. Geol. 114, 206–221.
Eldredge, S., Van der Voo, R., 1988. Paleomagnetic study of thrust sheet rotations in the Helena and Wyoming salients of the northern Rocky Mountains. In: Schmidt, C.J., Perry, W.J. Jr. (Eds.), Interaction of the Rocky Mountain Foreland and the Cordilleran Thrust Belt, vol. 171. Geological Society of America Memoir, pp. 319–332.
Ellis, S., Schreurs, G., Panien, M., 2004. Comparisons between analogue and numerical models of thrust wedge development. J. Struct. Geol. 26, 1659–1675. https://doi.org/10.1016/j.jsg.2004.02.012.
Farzipour-Saein, A., Koyi, H., 2014. Effect of lateral thickness variation of an intermediate decollement onthe propagation of deformation front in the Lurestan and Izeh zones ofthe Zagros fold-thrust belt, insights from analogue modeling. J. Struct. Geol. 65, 17–32. http://dx.doi.org/10.1016/j.jsg.2014.03.004.
Fernández, O., Beamud, E., Muñoz, J.A., Dinarés-Turell, J., Poblet, J., 2003. Distribución de las rotaciones paleomagnéticas en los anticlinales de Boltaña y Añisclo (Pirineos Centrales). MAGIBER II, Coimbra.
Fernández, O., Muñoz, J.A., Arbués, P., Falivene, O., 2012. 3D structure and evolution of an oblique system of relaying folds: the Ainsa basin (Spanish Pyrenees). Journal of the Geological Society, London 169, 545–559.
Ferrer, O., Carola, E., McClay, K., Bufaliza, N., 2022. Analog modeling of domino-style extensional basement fault systems with pre-kinematic salt. AAPG (Am. Assoc. Pet. Geol.) Bull. https://doi.org/10.1306/08072221188, 2022.
Fukao, Y., Yamaoka, K., Sakurai, T., 1987. Spherical shell tectonics: buckling of subducting lithosphere. Phys. Earth Planet. In. 45 (1), 59–67.
García-Senz, J., 2002. Cuencas extensivas del cretácico inferior en los Pirineos centrales, formación y subsecuente inversión. PhD Thesis. Universitat de Barcelona, Barcelona, p. 310.
Granado, P., Santolaria, P., Muñoz, J.A., 2023. Interplay of downbuilding and gliding in salt-bearing rifted margins: insights from analogue modelling and natural case studies. AAPG (Am. Assoc. Pet. Geol.) Bull. https://doi.org/10.1306/08072221203 (in press).
Graveleau, F., Malavieille, J., Dominguez, S., 2012. Experimental modelling of orogenic wedges: a review. Tectonophysics 538–540, 1–66.
Gutiérrez-Alonso, G., Johnston, S.T., Weil, A.B., Pastor-Galán, D., Fernández-Suárez, J., 2012. Buckling an orogen: the cantabrian orocline. GSA Today (Geol. Soc. Am.) 22 (7), 4–9.
He, W.G., Shen, G.B., Wu, L., Li, S.H., Zhao, Y.W., 2022. Deformational in curved fold-and-thrust belts: as a function of backstop shape and basal friction: insights from analogue modeling and application to the Pamir salient, Hindu Kush region. J. Struct. Geol. 162, 104680 https://doi.org/10.1016/j.jsg.2022.104680.
Hindle, D., Burkhard, M., 1999. Strain, displacement and rotation associated with the formation of curvature in fold belts; the example of the Jura arc. J. Struct. Geol. 21 (8), 1089–1101.
Hindle, D., Besson, O., Burkhard, M., 2000. A model of displacement and strain for arc-shaped mountain belts applied to the Jura arc. J. Struct. Geol. 22 (9), 1285–1296.
Hubbert, M.K., 1937. Theory of scale models as applied to the study of geologic structures. Geol. Soc. Am. Bull. 48, 1459–1519.
Hubbert, M.K., 1951. Mechanical basis for certain familiar geologic structures. Bull. Geol. Soc. Am. 62 (4), 355–372.
Izquierdo-Llavall, E., Casas Sainz, A., 2012. Influence of along-strike thickness variations in the detachment level on the geometry of thrust systems: preliminary analogue models. Geotemas 13, 521–524, 2012.
Jammes, S., Lavier, L., Manatschal, G., 2010. Extreme crustal thinning in the bay of biscay and the western Pyrenees: from observations to modeling. G-cubed 11 (10). https://doi.org/10.1029/2010GC003218.
Jammes, S., Huismans, R.S., Muñoz, J.A., 2014. Lateral variation in structural style of mountain building: controls of rheological and rift inheritance. Terra. Nova 26 (3), 201–207.
Jiménez-Bonilla, A., Crespo-Blanc, A., Balanyá, J.C., Expósito, I., Díaz-Azpiroz, M., 2020. Analog models of foldfold-and-thrust wedges in progressive arcs: a comparison with the Gibraltar arc external wedge. Front. Earth Sci. 8, 72. https://doi.org/10.3389/feart.2020.00072.
Jiménez-Bonilla, A., Expósito-Ramos, I., Díaz-Azpíroz, M., Balanyá, J.C., Crespo-Blanc, A., 2022. Strain partitioning and localization due to detachment heterogeneities in fold-and-thrust belts of progressive arcs: results from analog modeling. Tectonics 41, e2021TC006955. https://doi.org/10.1029/2021TC006955.
Joudaki, M., Farzipour-Saein, A., Nilfouroushan, F., 2016. Kinematics and surface fracture pattern of the Anaran basement fault zone in NW of the Zagros fold–thrust belt. Int. J. Earth Sci. 105, 869–883.
Keep, M., 2000. Models of lithospheric-scale deformation during plate collision: effects of indentor shape and lithospheric thickness. Tectonophysics 326 (3), 203–216.
Klinkmüller, M., Schreurs, G., Rosenau, M., Kemnitz, H., 2016. Properties of granular analogue materials: a community wide survey. Tectonophysics 684, 23–38.
Konstantinovsky, A.A., 2007. Structure and geodynamics of the Verkhoyansk fold-thrust belt. Geotectonics 41 (5), 337–354.
Koyi, H., Sans, M., 2006. Deformation transfer in viscous detachments: comparison of sandbox models to the South Pyrenean Triangle Zone. In: Buiter, S.J.H., Schreurs, G. (Eds.), 2006. Analogue and Numerical Modelling of Crustal-Scale Processes, vol. 253. Geological Society, London, Special Publications, pp. 117–134.
Krantz, R.W., 1991. Measurements of friction coefficients and cohesion for faulting and fault reactivation in laboratory models using sand and sand mixtures. Tectonophysics 188, 203–207.
Lacombe, O., Bellahsen, N., Mouthereau, F., 2011. Fracture patterns in the Zagros Simply Folded Belt (Fars, Iran): constraints on early collisional tectonic history and role of basement faults. Geol. Mag. 148 (5–6), 940–963.
Leturmy, P., Mugnier, J.L., Vinour, P., Baby, P., Colletta, B., Chabron, E., 2000. Piggyback basin development above a thin-skinned thrust belt with two detachment levels as a function of interactions between tectonic and superficial mass transfer: the case of the Subandean Zone (Bolivia). Tectonophysics 320 (1), 45–67.
Li, J., Mitra, S., 2017. Geometry and evolution of fold-thrust structures at the boundaries between frictional and ductile detachments. Mar. Petrol. Geol. 85, 16–34. https://doi.org/10.1016/j.marpetgeo.2017.04.011.
Lickorish, W.H., Ford, M., Bürgisser, J., Cobbold, P.R., 2002. Arcuate thrust systems in sandbox experiments: a comparison to the external arcs of the Western Alps. GSA Bull. 114 (9), 1089–1107. https://doi.org/10.1130/0016-7606(2002)114%3C1089:ATSISE%3E2.0.CO;2.
Liesa, C.L., Simón, J.L., 2009. Evolution of intraplate stress fields under multiple remote compressions; the case of the Iberian Chain (NE Spain). Tectonophysics 474, 144–159. https://doi.org/10.1016/j.tecto.2009.02.002.
Likerman, J., Burlando, J.F., Cristallini, E.O., Ghiglione, M.C., 2013. Along-strike structural variations in the Southern Patagonian Andes: insights from physical modeling. Tectonophysics 590, 106–120.
Lin, H., Wang, Z., Zhang, T., Qiao, X., 1992. Cambrian in Tarim. In: Zhiyi, Zhou, Peiji, Chen (Eds.), Biostratigraphy and Geological Evolution of Tarim. Science, Beijing, pp. 9–61.
Linzer, H.G., 1996. Kinematics of retreating subduction along the Carpathian arc, Romania. Geology 24 (2), 167–170.
Linzer, H.G., Frisch, W., Zweigel, P., Girbacea, R., Hann, H.P., Moser, F., 1998. Kinematic evolution of the Romanian Carpathians. Tectonophysics 297 (1), 133–156.
Liu, H., McClay, K.R., Powell, D., 1992. Physical models of thrust wedges. In: McClay, K. R. (Ed.), Thrust Tectonics. Chapman and Hall, London, pp. 71–81.
Lohrmann, J., Kukowski, N., Adam, J., Oncken, O., 2003. The impact of analogue material properties on the geometry, kinematics and dynamics of convergent sand wedges. J. Struct. Geol. 25, 1961, 1711.
Lu, C.Y., Jeng, F.S., Chang, K.J., Jian, W.T., 1998. Impact of basement high on the structure and kinematics of the western Taiwan thrust wedge: insights from sandbox models. Terr. Atmos. Ocean Sci. 9 (3), 533–550.
Luján, M., Storti, F., Balanyá, J.-C., Crespo-Blanc, A., Rossetti, F., 2003. Role of décollement material with different rheological properties in the structure of the Aljibe thrust imbricate (Flysch Trough, Gibraltar Arc): an analogue modelling approach. J. Struct. Geol. 25, 867–881.
Macedo, J., Marshak, S., 1999. Controls on the geometry of fold-thrust belt salients. Geol. Soc. Am. Bull. 111 (12), 1808–1822.
Mandl, G., De Jong, L.N.J., Maltha, A., 1977. Shear zones in granular material. Rock Mech. 9, 98–144.
Marques, F.O., Cobbold, P.R., 2002. Topography as a major factor in the development of arcuate thrust belts: insights from sandbox experiments. Tectonophysics 348, 247–268. https://doi.org/10.1016/S0040-1951(02)00077-X.
Marshak, S., 2004. Salients, recesses, arcs, Oroclines, and Syntaxes A review of ideas concerning the formation of map-view curves in fold-thrust beltsMcClay, K.R. (Ed.), In: Thrust Tectonics and Hydrocarbon Systems: AAPG Memoir, 82, pp. 133–158.
Marshak, S., Wilkerson, M.S., 1992. Effect of overburden thickness on thrust belt geometry and development. Tectonics 11, 560–566.
Marshak, S., Wilkerson, M.S., Hsui, A.T., 1992. Generation of curved fold-thrust belts: insight from simple physical and analytical models. In: McClay, K.R. (Ed.), Thrust Tectonics. Chapman and Hall, London, pp. 83–92.
McCaig, A.M., McClelland, E., 1992. Palaeomagnetic techniques applied to thrust belts. In: McClay, K.R. (Ed.), Thrust Tectonics. Chapman and Hall, London, pp. 209–216.
McClay, K., 1992. Glossary. In: McClay, K.R. (Ed.), Thrust Tectonics. Chapman and Hall, London, pp. 419–433.
Merten, S., Smit, W.G., Nieuwland, D.A., Rondeel, H.E., 2006. Analogue modelling of a reactivated, basement controlled strike-slip zone, Sierra de Albarracín, Spain: application of sandbox modelling to polyphase deformation. Geological Society, London, Special Publications 253 (1), 135–152.
Miró, J., Ferrer, O., Muñoz, J.A., Manastchal, G., 2022. Role of Inheritance during Tectonic Inversion of a Rift System in a Thick to Thin-Skin Transition: Analogue

Modelling and Application to the Pyrenean – Biscay System. https://doi.org/10.5194/egusphere-2022-1175. EGUsphere [preprint].
Mobasher, K., Babaie, H.A., 2008. Kinematic significance of fold-and fault-related fracture systems in the Zagros mountains, southern Iran. Tectonophysics 451 (1), 156–169.
Mochales, T., Casas, A.M., Pueyo, E.L., Barnolas, A., 2012. Rotational velocity for oblique structures (Boltaña anticline, Southern Pyrenees). J. Struct. Geol. 35, 2–16.
Molnar, P., Tapponnier, P., 1975. Cenozoic tectonics of Asia: effects of a continental collision. Science 189 (4201), 419–426.
Montanari, D., Agostini, A., Bonini, M., Corti, G., Del Ventisette, C., 2017. The use of empirical methods for testing granular materials in analogue modelling. Materials 10 (6), 635. https://doi.org/10.3390/ma10060635.
Mora, A., Parra, M., Strecker, M.R., Sobel, E.R., Zeilinger, G., Jaramillo, C., Da Silva, S.F., Blanco, M., 2010. The eastern foothills of the Eastern Cordillera of Colombia: an example of multiple factors controlling structural styles and active tectonics. GSA Bulletin 122 (11–12), 1846–1864.
Morley, C.K., 1987. Lateral and vertical changes of deformation style in the osen-røa thrust sheet, Oslo region. J. Struct. Geol. 9 (3), 331–343.
Morley, C., 2009. Geometry of an oblique thrust fault zone in a deepwater fold belt from 3D seismic data. J. Struct. Geol. 31, 1540–1555.
Muñoz, J.A., 1992. Evolution of a continental collision belt: ECORS-Pyrenees crustal balanced cross-section. In: McClay, K.R. (Ed.), Thrust Tectonics. Chapman and Hall, London, pp. 235–246.
Muñoz, J.A., Beamud, E., Fernández, O., Arbués, P., Dinarès-Turell, J., Poblet, J., 2013. The Ainsa Fold and thrust oblique zone of the central Pyrenees: kinematics of a curved contractional system from paleomagnetic and structural data. Tectonics 32 (5), 1142–1175.
Muñoz, J.A., Mencos, J., Roca, E., Carrera, N., Gratacos, O., Ferrer, O., Fernández, O., 2018. The structure of the South-Central Pyrenean fold and thrust belt as constrained by subsurface data. Geol. Acta: Int. Earth Sci. J. 16 (4), 439–460. https://doi.org/10.1344/GeologicaActa2018.16.4.7.
Oliva-Urcia, B., Pueyo, E.L., 2007. Gradient of shortening and vertical-axis rotations in the Southern Pyrenees (Spain), insights from a synthesis of paleomagnetic data. Rev. Soc. Geol. Esp. 20, 105–118.
Panien, M., Schreurs, G., Pfiffner, A., 2006. Mechanical behaviour of granular materials used in analogue modelling: insights from grain characterization, ring-shear tests and analogue experiments. J. Struct. Geol. 28, 1710–1724.
Philippe, 1995. Rampes latérales et zones de transfert dans les chaînes plissées: géométrie, conditions de formation et pièges structuraux associés. PhD Thesis. Université de Savoie.
Philippe, Y., Deville, E., Mascle, A., 1998. In: Mascle, A., Puigdefábregas, C., Luterbacher, H.P., Fernández, M. (Eds.), Thin-skinned Inversion Tectonics at Oblique Basin Margins: Example of the Western Vercors and Chartreuse Subalpine Massifs (SE France), Cenozoic Foreland Basins of Western Europe, vol. 134. Geological Society Special Publications, pp. 1–28.
Pla, O., Izquierdo-Llavall, E., Roca, E., Ferrer, O., Gratacós, Ò., Muñoz, J.A., 2018. Control of syn-tectonic sedimentation and décollement rheology in the geometry and evolution of the Kuqa fold-and-thrust belt (NW China). In: Results from Analogue Modelling. GeoMod2018, Barcelona.
Pla, O., Roca, E., Xie, H., Izquierdo-Llavall, E., Muñoz, J.A., Rowan, M.G., et al., 2019. Influence of Syntectonic sedimentation and Décollement rheology on the geometry and evolution of Orogenic wedges: analog modeling of the Kuqa fold-and-Thrust Belt (NW China). Tectonics 38 (8), 2727–2755.
Pueyo, E.L., Mauritsch, H.J., Gawlick, H.J., Scholger, R., Frisch, W., 2007. New evidence for block and thrust sheet rotations in the central northern Calcareous Alps deduced from two pervasive remagnetization events. Tectonics 26 (5). https://doi.org/10.1029/2006TC001965.
Ramberg, H., 1967. Gravity, Deformation, and the Earth's Crust in Theory, Experiments and Geological Applications. 1st Edition. Academic-Press, London, New York.
Ravaglia, A., Turrini, C., Seno, S., 2004. Mechanical stratigraphy as a factor controlling the development of a sandbox transfer zone: a three-dimensional analysis. J. Struct. Geol. 26, 2269–2283.
Ravaglia, A., Seno, S., Toscani, G., Fantoni, R., 2006. Mesozoic extension controlling the Southern Alps thrust front geometry under the Po Plain, Italy: insights from sandbox models. J. Struct. Geol. 28, 2084–2096.
Reiter, K., Kukowski, N., Ratschbacher, L., 2011. The interaction of two indenters in analogue experiments and implications for curved fold-and-thrust belts. Earth Planet Sci. Lett. 302 (1), 132–146.
Replumaz, A., Tapponnier, P., 2003. Reconstruction of the deformed collision zone between India and Asia by backward motion of lithospheric blocks. J. Geophys. Res. Solid Earth 108 (B6).
Rodríguez-Pintó, A., Pueyo, E.L., Calvín, P., Sánchez, E., Ramajo, J., Casas, A.M., Ramón, M.J., Pocoví, A., Barnolas, A., Román, T., 2016. Rotational kinematics of a curved fold: the Balzes anticline (Southern Pyrenees). Tectonophysics 677–678, 171–189.
Román-Berdiel, T., Casas, A.M., Pueyo, E.L., Peiro, A., Soto, R., Pohlenz, A., Warsitzka, M., Rosenau, M., 2019. Ring Shear Test Data of Quartz Sand and Colored Quartz Sand Used for Analogue Experiments in the Analogue Modelling Laboratory of the University of Zaragoza, Spain (EPOS TNA Call 2017). GFZ Data Services. https://doi.org/10.5880/fidgeo.2019.025.
Rosenberg, C.L., Brun, J.P., Cagnard, F., Gapais, D., 2007. Oblique indentation in the Eastern Alps: insights from laboratory experiments. Tectonics 26 (2). https://doi.org/10.1029/2006TC001960.
Rosenau, M., Pohlenz, A., Kemnitz, H., Warsitzka, M., 2018. Ring-shear Test Data of Quartz Sand G23 Used for Analogue Experiments in the Helmholtz Laboratory for Tectonic Modelling (HelTec) at the GFZ German Research Centre for Geosciences in Potsdam. GFZ Data Services. https://doi.org/10.5880/GFZ.4.1.2019.004.
Rowan, M.G., Vendeville, B.C., 2006. Foldbelts with early salt withdrawal and diapirism: physical model and examples from the northern Gulf of Mexico and the Flinders Ranges, Australia. Mar. Petrol. Geol. 23, 871–891.
Rowan, M.G., 2014. Passive-margin salt basins: hyperextension, evaporite deposition, and salt tectonics. Basin Res. 26 (1), 154–182. https://doi.org/10.1111/bre.12043, 10.1111/bre.12043.
Rudolf, M., Boutelier, D., Rosenau, M., Schreurs, G., Oncken, O., 2016. Rheological benchmark of silicone oils used for analog modeling of short- and long-term lithospheric deformation. Tectonophysics 684, 12–22.
Sadeghi, S., Storti, F., Yassaghi, A., Nestola, Y., Cavozzi, C., 2016. Experimental deformation partitioning in obliquely converging orogens with lateral variations of basal décollement rheology: inferences for NW Zagros, Iran. Tectonophysics 693, 223–238.
Sans, M., 2003. From thrust tectonics to diapirism. The role of evaporites in the kinematic evolution of the eastern South Pyrenean front. Geol. Acta 1, 239–259.
Santolaria, P., Harris, L., Casas, A., Soto, R., 2014. Fold-and-thrust belt evolution influenced by along and across strike thickness variations: new insights from brittle-ductile centrifuge analogue models. In: Geophysical Research Abstracts 16. EGU General Assembly, pp. EGU2014–15315.
Santolaria, P., Vendeville, B.C., Graveleau, F., Soto, R., 2015. Double evaporitic décollements: influence of pinch-out overlapping in experimental thrust wedges. J. Struct. Geol. 76, 35–51.
Santolaria, P., Ferrer, O., Rowan, M.G., Snidero, M., Carrera, N., Granado, P., et al., 2021a. Influence of preexisting salt diapirs during thrust wedge evolution and secondary welding: insights from analog modeling. J. Struct. Geol. 149, 104374 https://doi.org/10.1016/j.jsg.2021.104374.
Santolaria, P., Granado, P., Carrera, N., Schneider, C.L., Ferrer, O., Snidero, M., et al., 2021b. From downbuilding to contractional reactivation of salt-sediment systems: insights from analog modeling. Tectonophysics 918, 229078. https://doi.org/10.1016/j.tecto.2021.229078.
Santolaria, P., Harris, L.B., Casas, A.M., Soto, R., 2022. Influence of décollement-cover thickness variations in fold-and-thrust belts: insights from centrifuge analog modeling. J. Struct. Geol. 163, 104704 https://doi.org/10.1016/j.jsg.2022.104704.
Schori, M., Zwaan, F., Schreurs, G., Mosar, J., 2021. Pre-existing basement faults controlling deformation in the Jura mountains fold-and-thrust belt: insights from analogue models. Tectonophysics 814, 228980. https://doi.org/10.1016/j.tecto.2021.228980.
Schellart, W.P., 2000. Shear test results for cohesion and friction coefficients for different granular materials: scaling implications for their usage in analogue modelling. Tectonophysics 324, 1–16.
Schellart, W.P., Strak, V., 2016. A review of analogue modelling of geodynamic processes: approaches, scaling, materials and quantification, with an application to subduction experiments. J. Geodyn. 100, 7–32.
Schreurs, G., Hänni, R., Vock, P., 2001. Four-dimensional Analysis of Analog Models: Experiments on Transfer Zones in Fold and Thrust Belts, vol. 193. Geological Society of America, Memoir, pp. 179–190.
Seely, D.R., 1977. The significance of landward vergence and oblique structural trends on trench inner slopes. In: Talwani, M. y Pitman (Ed.), Island Arcs. Deep Sea Trenches and Back-Arc Basins. W.C. American Geophysical Union, Washington, pp. 187–198.
Smit, J.H.W., Brun, J.P., Soukoutis, D., 2003. Deformation of brittle–ductile thrust wedges in experiments and nature. J. Geophys. Res. 108 (B10), 2480. https://doi.org/10.1029/2002JB002190.
Sobel, E.R., Chen, J., Schoenbohm, L.M., Thiede, R., Stockli, D.F., Sudo, M., Strecker, M. R., 2013. Oceanic-style subduction controls late Cenozoic deformation of the Northern Pamir orogeny. Earth Planet Sci. Lett. 363, 204–218. https://doi.org/10.1016/j.epsl.2012.12.009.
Soto, R., Casas, A.M., 2001. Geometría y cinemática de las estructuras norte-sur de la Cuenca de Aínsa. Rev. Soc. Geol. Espana 14 (3–4), 199–211.
Soto, R., Casas, A.M., Storti, F., Faccenna, C., 2002. Role of lateral thickness variations on the development of oblique structures at the Western end of the South Pyrenean Central Unit. Tectonophysics 350 (3), 215–235.
Soto, R., Storti, F., Casas, A.M., Faccenna, C., 2003. Influence of along-strike pre-orogenic sedimentary tapering on the internal architecture of experimental thrust wedges. Geol. Mag. 140 (3), 253–264.
Soto, R., Casas-Sainz, A.M., Pueyo, E.L., 2006a. Along-strike variation of orogenic wedges associated with vertical-axis rotations. J. Geophys. Res. 111 (B10402) https://doi.org/10.1029/2005JB004201.
Soto, R., Storti, F., Casas-Sainz, A.M., 2006b. Impact of backstop thickness lateral variations on the tectonic architecture of orogens: insights from sandbox analogue modeling and application to the Pyrenees. Tectonics 25 (2).
Soto, R., Vendeville, B., Graveleau, F., 2020. Interaction between perpendicularly-trending thrust wedges and its impact on foreland deformation: insights from analogue modelling. Tectonophysics 786, 228462. https://doi.org/10.1016/j.tecto.2020.228462.
Soto, R., Clariana, P., Ayala, C., Rey-Moral, C., Casas-Sainz, M., A, M., Román-Berdiel, T., Margalef, A., Rubio, F., Oliva-Urcia, B., Pueyo, L., E, L., Martín-León, J., Beamud, E., 2022. Assessing the internal uppermost crustal structure of the central Pyrenees by gravity-constrained cross sections. Tectonics 41 (8), e2021TC007009.
Souloumiac, P., Maillot, B., Leroy, Y.M., 2012. Bias due to side wall friction in sand box experiments. J. Struct. Geol. 35, 90–101. https://doi.org/10.1016/j.jsg.2011.11.002.
Speed, R., Westbrook, G., Mascle, A., Biju-Duval, B., Ladd, J., Saunders, J., Stein, S., Schoonmaker, J., Moore, J., 1984. In: Speed, R.C., Westbrook, G.F. (Eds.), Lesser

Antilles Arc and Adjacent Terranes Ocean Margin Drilling Program, Regional Atlas Series, Atlas 10, 27 Sheets, Marine Science Interiors Massachusetts: Woods Hole.
Storti, F., Salvini, F., McClay, K., 2000. Synchronous and velocity-partitioned thrusting and thrust polarity reversal in experimentally produced, doubly-vergent thrust wedges; implications for natural orogens. Tectonics 19 (2), 378–396.
Storti, F., Marín, R.S., Rossetti, F., Sainz, A.C., 2007. Evolution of experimental thrust wedges accreted from along-strike tapered, silicone-floored multilayers. J. Geol. Soc. 164 (1), 73–85.
Storti, F., McClay, K., 1995. Influence of syntectonic sedimentation on thrust wedges in analogue models. Geology 23 (11), 999–1002. https://doi.org/10.1130/0091-7613(1995)023<0999:iossot>2.3.co;2.
Sun, C., Jia, D., Yin, H., Chen, Z., Li, Z., Shen, L., Wei, D., Li, Y., Yan, B., Wang, M., Fang, S., Cui, J., 2016. Sandbox modeling of evolving thrust wedges with different preexisting topographic relief: implications for the Longmen Shan thrust belt, eastern Tibet. J. Geophys. Res. Solid Earth 121, 4591–4614.
Sussman, A.J., Butler, R.F., Dinarès-Turell, J., Vergés, J., 2004. Vertical-axis rotation of a foreland fold and implications for orogenic curvature: an example from the Southern Pyrenees, Spain. Earth Planet Sci. Lett. 218, 435–449.
Teixell, A., Muñoz, J.A., 2000. Evolución tectono-sedimentaria del Pirineo meridional durante el Terciario: una síntesis basada en la transversal del río Noguera Ribagorçana. Rev. Soc. Geol. España 13, 295–316.
Ter Borgh, M.M., Oldenhuis, R., Biermann, C., Smit, J.H.W., Sokoutis, D., 2011. The effects of basement ramps on deformation of the Prebetics (Spain): a combined field and analogue modelling study. Tectonophysics 502 (1), 62–74.
Thomas, W.A., 1986. A Paleozoic synsedimentary structure in the Appalachian fold-and-thrust belt in Alabama. In: McDowell, R.C., Glover, L., III., Virginia (Eds.), The Lowry Volume: Studies in Appalachian Geology, vol. 12. Tech Dept. Geol. Sci. Mem., pp. 1–12
Thomas, W.A., 1990. Controls on locations of transverse zones in thrust belts. Eclogae Geol. Helv. 83, 727–744.
Thöny, W., Ortner, H., Scholger, R., 2006. Paleomagnetic evidence for large en-bloc rotations in the Eastern Alps during Neogene orogeny. Tectonophysics 414 (1), 169–189.
Tugend, J., Manatschal, G., Kusznir, N.J., Masini, E., Mohn, G., Thinon, I., 2014. Formation and deformation of hyperextended rift systems: insights from rift domain mapping in the Bay of Biscay-Pyrenees. Tectonics 33, 1239–1276. https://doi.org/10.1002/2014TC003529.
Turner, S.A., Cosgrove, J.W., Liu, J.G., 2010. Controls on lateral structural variability along the keping Shan thrust belt, SW tien Shan foreland, China. Geological Society, London, Special Publications 348 (1), 71–85.
Turner, S.A., Liu, J.G., Cosgrove, J.W., 2011. Structural evolution of the Piqiang Fault zone, NW Tarim Basin, China. J. Asian Earth Sci. 40 (1), 394–402.
Turrini, C., Ravaglia, A., Perotti, C.R., 2001. Compressional structures in a multilayered mechanical stratigraphy: insights from sandbox modeling with three-dimensional variations in basalgeometry and friction. In: Koyi, H.A., Mancktelow, N.S. (Eds.), Tectonic Modeling: A Volume in Honor of Hans Ramberg, vol. 193. Geological Society of America Memoir, Boulder, Colorado, pp. 153–178.
Valcárcel, M., Soto, R., Beaumud, E., Oliva-Urcia, B., Muñoz, J.A., Biete, C., 2015. Integration of palaeomagnetic data, basement-cover relationships and theoretical calculations to characterize the obliquity of the Altomira-Loranca structures (central Spain). Spec. Publ. Geol. Soc. Lond. 425 (1), 169–188.
Vendeville, B.C., Nilsen, K.T., 1995. Episodic growth of salt diapirs driven by horizontal shortening. In: Travis, C.J., Harrison, H., Hudec, M.R., Vendeville, B.C., Peel, F.J., Perkins, B.F. (Eds.), Salt, Sediment, and Hydrocarbons. SEPM Gulf Coast Section 16th Annual Research Foundation Conference, pp. 285–295.
Van der Werf, I., Schellart, W.P., Strak, V., van Agtmaal, L., Blankendal, R., 2023. Analogue modelling of the Ainsa oblique zone in the Southern Central Pyrenees, Spain. J. Struct. Geol. 177, 104964. https://doi.org/10.1016/j.jsg.2023.104964.
Vendeville, B.C., Pengcheng, T., Graveleau, F., Shaoying, H., Wang, X., 2017. How the presence of a salt décollement in the sedimentary cover influences the behavior of subsalt thrusts in fold-and-thrust belts. Bull. Soc. Geol. Fr. 188, 37.
Vidal-Royo, O., Koyi, H.A., Muñoz, J.A., 2009. Formation of orogen-perpendicular thrusts due to mechanical contrasts in the basal décollement in the Central External Sierras (Southern Pyrenees, Spain). J. Struct. Geol. 31 (5), 523–539.
Warsitzka, M., Závada, P., Pohlenz, A., Rosenau, M., 2019. Ring-shear Test Data of Quartz Sand Used for Analogue Experiments in the Laboratory of the Institute of Geophysics of the Czech Academy of Science. GFZ Data Services. https://doi.org/10.5880/GFZ.4.1.2019.008.
Weijermars, R., 1986. Finite strain of laminar flows can be visualized in SGM36-polymer. Naturwissenschafen 73, 33–34.
Weijermars, R., Schmeling, H., 1986. Scaling of Newtonian and non-Newtonian fluid dynamics without inertia for quantitative modelling of rock flow due to gravity (including the concept of rheological similarity). Phys. Earth Planet. In. 43, 316–330.
Weil, A.B., Sussman, A.J., 2004. Classifying curved orogens based on timing relationships between structural development and vertical-axis rotations. Geol. Soc. Am. 383, 1–15. https://doi.org/10.1130/0-8137-2383-3(2004)383[1:CCOBOT]2.0.CO;2.
Willingshofer, E., Sokoutis, D., Beekman, F., Schönebeck, J.-M., Warsitzka, M., Rosenau, M., 2018. Ring Shear Test Data of Feldspar Sand and Quartz Sand Used in the Tectonic Laboratory (TecLab) at Utrecht University for Experimental Earth Science Applications. GFZ Data Services. https://doi.org/10.5880/fidgeo.2018.072.
Wilson, E.P., Granado, P., Santolaria, P., Ferrer, O., Muñoz, J.A., 2023. Inversion of Transfer Zones in Salt-Bearing Extensional Systems: Insights from Analogue Modeling. https://doi.org/10.5194/egusphere-2022-1461. EGUsphere [preprint].
Wu, Jonathan E., McClay, Ken R., 2011. Two-dimensional analog modeling of fold and thrust belts: dynamic interactions with syncontractional sedimentation and erosion. In: McClay, K., Shaw, J.H., Suppe, J. (Eds.), Thrust Fault-Related Folding: AAPG Memoir 94, pp. 301–333.
Yamaoka, K., Fukao, Y., Kumazawa, M., 1986. Spherical shell tectonics: effects of sphericity and inextensibility on the geometry of the descending lithosphere. Rev. Geophys. 24 (1), 27–53.
Yonkee, W.A., Weil, A.B., 2015. Tectonic evolution of the sevier and laramide belts within the North American cordillera orogenic system. Earth Sci. Rev. 150, 531–593.
Zwaan, F., Schreurs, G., Gentzmann, R., Warsitzka, M., Rosenau, M., 2018. Ring-shear Test Data of Quartz Sand from the Tectonic Modelling Lab of the University of Bern (CH). GFZ Data Services. https://doi.org/10.5880/fidgeo.2018.028.
Zweigel, P., 1998. Arcuate accretionary wedge formation at convex plate margin corners: results of sandbox analogue experiments. J. Struct. Geol. 20 (12), 1597–1609.
Zweigel, P., Ratschbacher, L., Frisch, W., 1998. Kinematics of an arcuate fold-thrust belt; the southern Eastern Carpathians (Romania). Tectonophysics 297 (1–4), 177–208.